ISSN: 2737-8071

International Journal of Engineering and Applied Physics

Volume No. 4
Issue No. 1
January - April 2024

ENRICHED PUBLICATIONS PVT.LTD

JE - 18,Gupta Colony, Khirki Extn,
Malviya Nagar, New Delhi - 110017.
E- Mail: info@enrichedpublication.com
Phone :- +91-8877340707

ISSN: 2737-8071

International Journal of Engineering and Applied Physics

About the Journal

All articles in the International Journal of Engineering and Applied Physics will be processed by the editor through the Online Journal System (OJS), and the author can monitor the entire process in the member's area. The articles published in The International Journal of Engineering and Applied Physics, soft copy form are available as open access for educational, research, and library purposes, and beyond that purpose, the editorial board of The International Journal of Engineering and Applied Physics is not responsible for copyright infringement.

ISSN: 2737-8071

International Journal of Engineering and Applied Physics

ISSN: 2737-8071

International Journal of Engineering and Applied Physics

(Volume No. 4, Issue No. 1, January - April 2024)

Contents

Smart speed bump for mechanical energy harvesting from roads

Chouaib ENNAWAOUI, Abdelowahed HAJJAJI, Abdessamad ELBALLOUTI, Azeddine AZIM

Laboratory of Engineering Sciences for Energy (LabSIPE)

National School of Applied Sciences EL Jadida, Chouaib Doukkali University

A B S T R A C T

A great deal of research has in recent years been carried out on harvesting energy using smart systems. Harvesting energy from the ambient environment has become an emerging technology for many applications, ranging from portable electric devices to renewable energy. This article constitutes a synthesis of work carried out within the framework of a study on systems for energy harvesting. The objective of the project was to design an intelligent retarder system. The advantage of the energy recovery system is that it transforms the kinetic energy produced by the passage of vehicles on the retarder to electric energy using a mechanism. The powers involved in this context can go up to 46 kW/h.

Keywords:Smart speed bump, Electrical energy, Mechanism, Energy harvesting.

1. INTRODUCTION

Generally, the production of electrical energy is done from fossil fuels (coal, oil, natural gas), and if these energies are clean and non-polluting, their production causes adverse effects on the environment, as well as these sources of energy are not renewable because they take millions of years to build up and because they are used much faster than the time needed to recreate reserves. In this context, several studies have been carried out to be able to recover electrical energy independently of these fossil fuels.

In 2008, the innowattech company tested a new technology called INNOWATTECH PIEZO ELECTRIC GENERATOR [1], is based on the principle of piezoelectricity [2-3]. The idea is to integrate piezoelectric single crystals in the road in order to recover and convert the mechanical energy produced by the passage of vehicles to electrical energy. One kilometer of this road allows innowatech to produce 400 kW per day and inject it into the public network. In 2009, the company sainsburg installed plates in their parking lot [4] in order to recover the kinetic energy by the passage of vehicles, but this time by a mechanism installed under the retarder. The objective of this installation is to supply the company's machines to reduce the loads due to energy, the power of which is generated by the retarder is 30 kW per hour. In the same year, inventor Peter Hughes proposed a new approach to kinetic energy harvesting [5], but this time with a new form of retarders. This invention is capable of supplying the surroundings with cylindrical breaks. Then, in 2011, the company New Energy Technology tested a retarder called MOTION POWER EXPRESS [6] composed of a mechanical-electrical conversion mechanism intended to supply a 150-foot screen during the day. Finally, in 2013, an Italian company asked the energy recovery market a speed bump [7] able to produce 6 GW per year with the passage of 400 vehicles per day, the throttle is equivalent to a high-power wind from 3MW.

Inspired by all these projects, this work is the update of speed bumps with a fairly simple and less expensive application, placed on motion transmission tools.

2. SYSTEM DESCRIPTION

The description relates to an energy harvesting retarder system. The interest of the system is to transform the kinetic energy produced by the passage of the vehicles on the retarder to an electric energy which can be used to supply the surroundings of the retarder by the mechanism able of producing a significant power of electricity, which the main use is public lighting to make sensors independent from the energy side.

Figure 1. Descriptive diagram of the intelligent retarder

3. FUNCTIONAL ANALYSIS OF THE SYSTEM

To define the expected functions of the model, we used the functional analysis. During this analysis, the product does not yet exist, a fortiori no solution is considered.

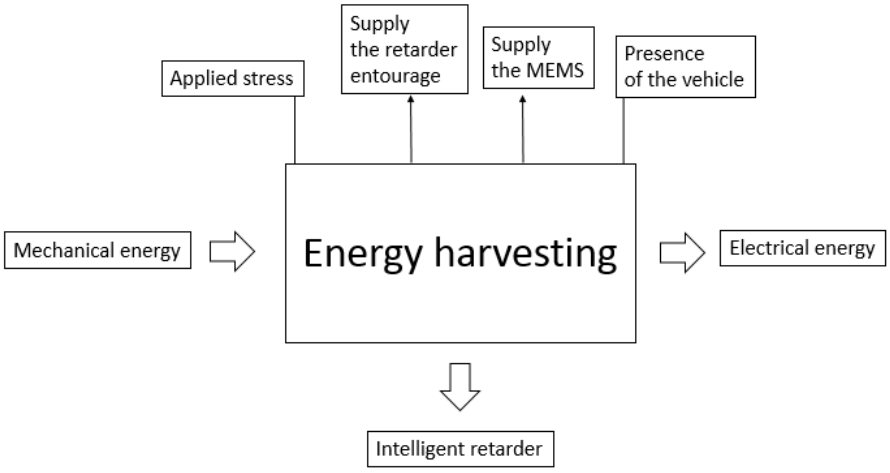

Figure 2. SADT diagram of the system

After having framed the context of the model, the SADT tool comes to allow us to define the various factors which will lead us to reach our goal which is to energy harvested by the use of a mechanical system. The energy recovered in this case is the mechanical energy produced by the passage of vehicles above the entrance to the overall system, but the technical functions and the associated solutions must be more detailed, and to do this we have recourse to the diagram of FAST To detail the functions and the technological solutions of the system, we have broken down the diagram FAST corresponds to the global system (figure 3).

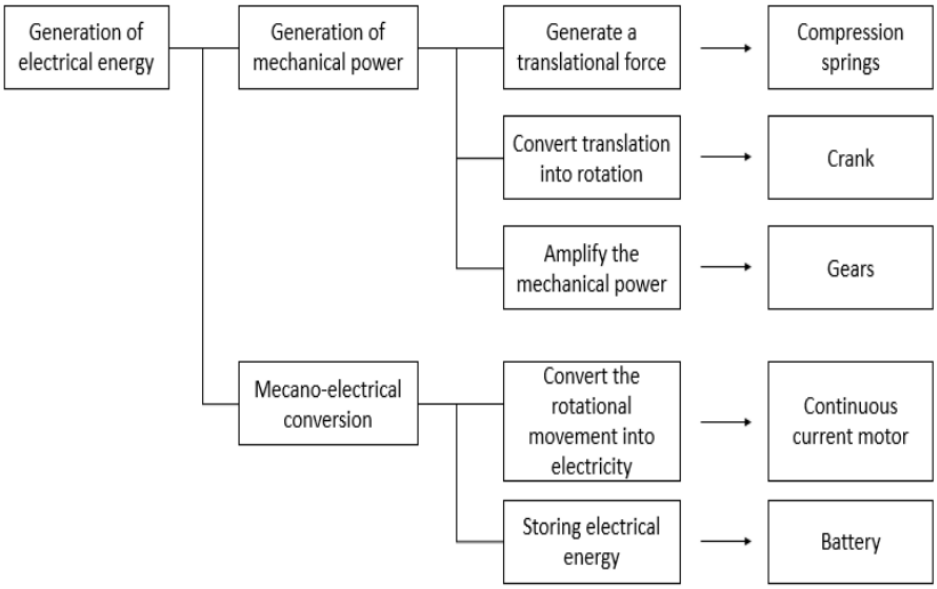

Figure 3. FAST diagram of the system

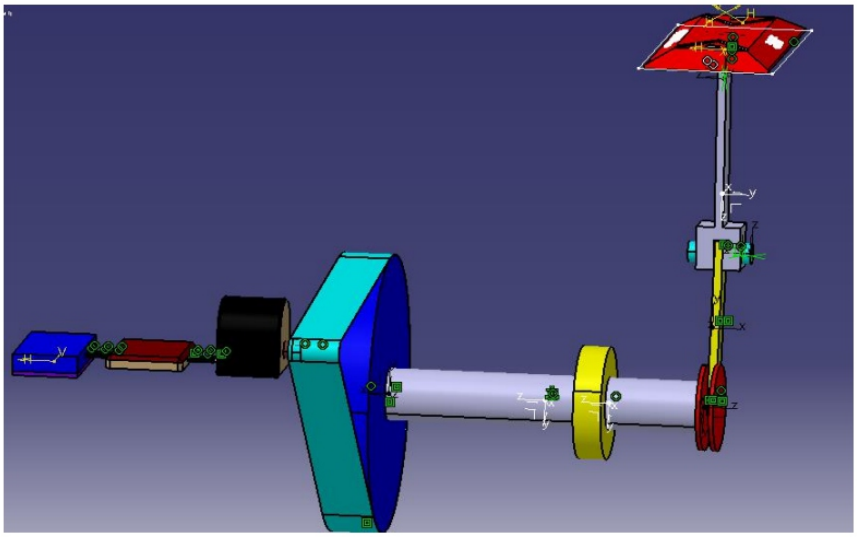

Figure 4. Global perspective of the system

4. SYSTEM COMPOSITIONS

4.1 The composition of the mechanical system:

The purpose of the mechanical composition of the mechanism is to generate a maximum of rotation for the supply of a direct current motor; and for proper operation, it has been proposed to use mechanical subsystems mentioned in figure 5.

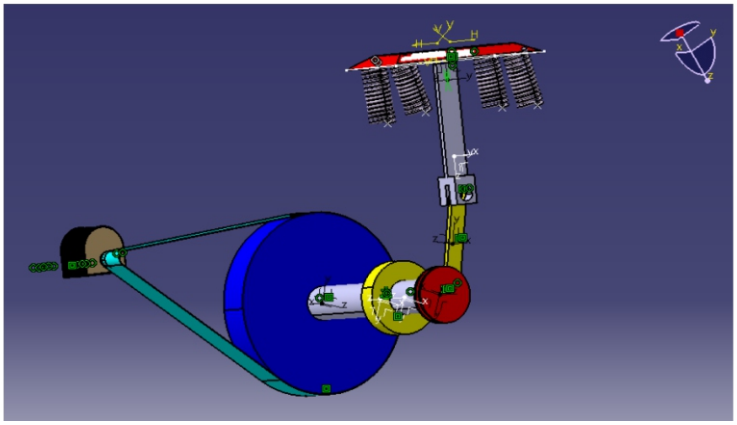

Figure 5. Mechanical part of the system

Compression springs: The mass of the vehicle running on the retarder must not exceed 50 Kg. The latter is supported by 5 springs which are distributed under the retarder, so each spring must withstand 1/5 of the overall force, m = 10 Kg.

Rod-crank: The connecting rod-crank system is a model of mechanism, which owes its name to the two parts that characterize it. It is, above all, a mechanical system for transforming movement.

Power multiplication system: After studying the power multiplication systems (pulley, belt, gear), we concluded that the gears will be more useful for our model, since they do not take up space compared to the belt pulley, on the other hand the latter will be very useful to us if we manage to carry out the project on a large scale given its output and its cost especially the synchronous belts. Less expensive, accessible, and above all, since they provide more advantages than disadvantages, parallel gears with helical teeth have a good multiplication system. Therefore, we only have sizing this system.

4.2 Electrical composition of the mechanism

The essential objective of the electrical composition of the mechanism is to convert mechanical energy into a form that is more usable, simple to store and which meets quality and safety standards. This electrical energy requires an installation made up of several well-chosen elements.

At the beginning, it is necessary to proceed by a general study of the whole system in order to choose and calculate the recovered power.

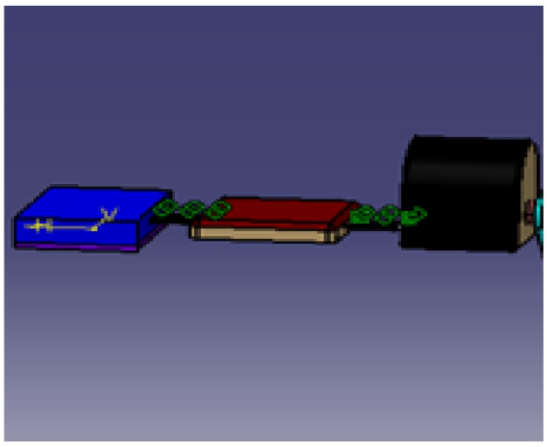

Figure 6. Overall drawing of the electrical part

The composition of the electrical part is summarized in the following elements:
A direct current machine is an electrical machine. It is an electromechanical converter allowing the bidirectional conversion of energy between an electrical installation carried by a direct current and a mechanical device. It is also called a dynamo.
The battery is used to supply the equipment which must remain energized (the surroundings of the retarder).

5. ENERGY BALANCE:

The number of teeth was chosen according to international standards and according to the type of gear used in the model.
Data: The force applied to the bearing surface F = 100N. The distance between the bearing surface and center of the connecting rod is d = 20 cm

Calculation of the power generated by the system:
Ce = F*d
Ce = 20 N.m
Cs = n 2 .Ce (-1) (We / Ws)
Cs = 1.73 N.m
Pa = Cs.Ws
Pa = 36.2 W
Pu = n1.Pu
Pu = 28.9W
With Ce, Cs, n2 , m, We, Ws, Pa, Pu and n1 respectively the input torque of the gear train, output torque of the gear train, efficiency of the gear train, number of contacts between the pinions, input speed of the gear train, output speed of the gear train, mechanical power absorbed, useful power and efficiency of the direct current motor (we estimated the losses at 20%) [9-11].
The following table gives the values of the power per hour as a function of the flow of the cars passing over the retarder.

Number of cars per hour	Power in kW/h
100	5.8
200	11.6
400	23.2
800	46.4

Table 1. Energy balance for the real system

With an easily available energy source, “road” energy recovery [8] would constitute a new source of clean and renewable energy. This system does not require any human intervention except preventive maintenance or battery change.

Conclusion

The works presented in our article allow the concept ion of a new system for the recovery of kinetic energy. Following our study, we were able to observe thanks to the system design that it is possible to make the mechanical-electrical conversion of the energy generated by the passage of vehicles on the retarders.We are therefore going to devote the next study to the production of the model, the marketing and the study and detailed analysis of the various organs of the system in order to be able to act directly and propose improvement actions.

References

[1] Z. Hongduo, L. Jianming and F. Pengcheng, ''A Review of Harvesting Green Energy from Road", Advanced Materials Research Vol. 723 pp 559-566, 2013.

[2] C. Ennawaoui, A.Hajjaji, A.Azim, and Y. Boughaleb, ''Theoretical modeling of power harvested by piezocellular polymers", Molecular Crystals and Liquid Crystals 628 (1): pp. 49-54, 2016.

[3] F. Belhora, A.Hajjaji, M.Mazroui, FZEl Fatnani, A.Rjafallah and D.Guyomar, ''Energy harvesting using hybridization of dielectric nanocomposites and electrets", Polym. Adv. Technol. 5 John Wiley & Sons, Ltd, 2015.

[4] L. Jaeyun and C. Bumkyoo, ''Development of a piezoelectric energy harvesting system for implementing wireless sensors on the tires. Energy Conversion and Management 78, 32–38, 2014.

[5] S. Chunhua, S. Gua ngqing, T. Yiyi, and T. Zhirong. A review on application of piezoelectric energy harvesting technology. Advanced Materials Research Vols. 516-517 pp 1481-148, 2012.

[6] C. Ennawaoui, , H. Lifi, A. Hajjaji, A. Elballouti, S. Laasri, & A. Azim, ''Mathematical modeling of mass spring's system: Hybrid speed bumps application for mechanical energy harvesting. Engineering Solid Mechanics", 7(1), 47-58, 2019.

[7] E. Ginelli, L. Daglio, ''Energyscapes: Developing a Multiscalar Systemic Approach to Assess the Environmental, Social and Economic Impact of Renewable Energy Systems on Landscape", Proceedings of the 2 nd ICAUD International Conference in Architecture and Urban Design Epoka University, Tirana, Albania, Paper No. 152, 2014.

[8] Z. Malki, C. Ennawaoui, A. Hajjaji, I. Najihi, M. Eljouad & Y. Boughaleb, ''Pedestrian crossing system for the mechanical energy harvesting using piezoelectric materials", In IOP Conference Series: Materials Science and Engineering (Vol. 948, No. 1, p. 012030). IOP Publishing, 2020.

[9] C. Ennawaoui, H.Lifi, A. Hajjaji, C. Samuel, M. Rguiti, S. Touhtouh & C. Courtois, ''Dielectric and mechanical optimization properties of porous poly (ethylene-co-vinyl acetate) copolymer films for pseudo-piezoelectric effect", Polymer Engineering & Science, 59(7), 1455-1461, 2019.

[10] C.Ennawaoui, H. Lifi, A. Hajjaji, , A. Elballouti S. Laasri & A. Azim, ''Mathematical modeling of mass spring's system: Hybrid speed bumps application for mechanical energy harvesting", Engineering Solid Mechanics, 7(1), 47-58, 2019.

[11] C. Ennawaoui, H. Lifi, A. Hajjaji, A. E. Azim, A. Elballouti & M. Rguiti. New System to Harvest Road Energy Using Piezoelectric Polymers. Sensor Letters, 16(1), 41-47, 2018

Harmonic analysis associated with the Weinstein type operator on Rd

Azzedine Achak1, Radouan Daher2, Najat Safouane3

1Ecole Suprieure d'Education et Formation. Universit Chouaib Doukkali, El Jadida Morocco

2,3Department of Mathematics, Faculty of Sciences An Chock. University of Hassan II Casablanca 20100, Morocco

A B S T R A C T

We consider the Weinstein type operator Δα,d on Rd. We build transmutation operators Rα which turn out to be transmutation operator between Δα,d and the Laplacian Δd. Using this transmutation operators and its dual tRα, we develop a new commutative harmonic analysis on Rdcorresponding to the operator Δα,d.

Keywords: Weinstein type operator, Generalized Weinstein, transform, Transmutation operator, Annihilating sets

1. INTRODUCTION

We consider the Weinstein operator on $Rd+ = Rd–1 \times [0, \infty[$ defined by

$$\Delta_\alpha = \sum_{i=1}^{d} \frac{\partial^2}{\partial x_i^2} + \frac{2\alpha+1}{x_d}\frac{\partial}{\partial x_d}, \quad \alpha > -\frac{1}{2}. \tag{1}$$

The Weinstein operator has several applications in pure and applied mathematics especially in fluid mechanics (cf. [3]). The harmonic analysis associated with the Weinstein operator is studied by Ben Nahia and Ben Salem (cf. [1, 2]). In particular the authors have introduced and studied the generalized Fourier transform associated with the Weinstein operator. This transform is called the Weinstein transform. Very recently, many authors have investigated the behavior of the Weinstein transform with respect to several problems already studied for the Fourier transform; for instance, Paley-Wiener theorems [6], the Bockner-Hecke theorem [4], uncertainty principles associated with the Weinstein transform [5]. In this paper we introduce the Weinstein type operator on *Rd* defined by

$$\Delta_{\alpha,d} f(x) = \sum_{i=1}^{d} \frac{\partial^2 f(x', x_d)}{\partial x_i^2} + \frac{2\alpha+1}{x_d}\left(\frac{\partial f(x', x_d)}{\partial x_d} - \frac{\partial f(x', 0)}{\partial x_d}\right)$$

where $\alpha > \frac{-1}{2}$, $x = (x', x_d) = (x_1, x_2, .., x_d) \in \mathbb{R}^d$. If $f(x', 0) = 0$ we regain the Weinstein operator defined by (1). Throughout this paper, we provide a new harmonic analysis on $\mathbb{R}^d$ corresponding to the Weinstein type operator $\Delta_{d,\alpha}$.

Let us now be more precise and describe our results. To do so, we need to introduce some notations. Throughout this paper, we denote by

- $a_\alpha = \dfrac{2\Gamma(\alpha+1)}{\sqrt{\pi}\Gamma(\alpha+\frac{1}{2})}$, $\alpha > \frac{-1}{2}$. $d\mu_\alpha(x) = |x_d|^{2\alpha+1} dx_d dx' = |x_d|^{2\alpha+1} dx_1 dx_2 ... dx_d$.
- $E(\mathbb{R}^d)$ (resp. $D(\mathbb{R}^d)$) the space of $\mathcal{C}^\infty$ functions on $\mathbb{R}^d$, (resp. with compact support).
- $L^p_\alpha(\mathbb{R}^d)$ the class of measurable functions f on $\mathbb{R}^d$ such that

$$\|f\|_{p,\alpha} = \left(\int_{\mathbb{R}^d} |f(x', x_d)|^p |x_d|^{2\alpha+1} dx' dx_d \right)^{\frac{1}{p}} < +\infty, \text{ if } p < +\infty.$$
$$\|f\|_{\infty} = ess \sup_{x \in \mathbb{R}^d} |f(x)| < +\infty, \text{ if } p = +\infty.$$

- $f_e(x) = \dfrac{f(x', x_d) + f(x', -x_d)}{2}$ and $f_o(x) = \dfrac{f(x', x_d) - f(x', -x_d)}{2}$.

We recapitulate some facts about the eigenfunction $\Phi_{\lambda,\alpha}$ related to the Weinstein operator Δ_α. For more details we refer to [1].

For all $(x, \lambda) \in \mathbb{R}^d \times \mathbb{C}^d$ the eigenfunction $\Phi_{\lambda,\alpha}$ related to the Weinstein operator Δ_α as defined by

$$\Phi_{\lambda,\alpha}(x) = a_\alpha e^{-i\langle x', \lambda' \rangle} j_\alpha(x_d \lambda_d), \tag{2}$$

where $j_\alpha(z) = \Gamma(\alpha+1) \sum_{n=0}^{+\infty} \dfrac{(-1)^n \left(\frac{z}{2}\right)^{2n}}{n! \Gamma(n+\alpha+1)}$.

As $j_\alpha(x_d \lambda_d) = a_\alpha \displaystyle\int_0^1 (1-t^2)^{\alpha-\frac{1}{2}} \cos(x_d \lambda_d t) dt$,
it follows that

$$\Phi_{\lambda,\alpha}(x) = a_\alpha e^{-i\langle x', \lambda' \rangle} \int_0^1 (1-t^2)^{\alpha-\frac{1}{2}} \cos(x_d \lambda_d t) dt.$$

We may now define the function $\Psi_{\lambda,\alpha}$ which is inspired by $\Phi_{\lambda,\alpha}$.
For all $(x, \lambda) \in \mathbb{R}^d \times \mathbb{C}^d$ we define the function $\Psi_{\lambda,\alpha}$ as follows

$$\Psi_{\lambda,\alpha}(x) = a_\alpha e^{-i\langle x', \lambda' \rangle} \int_0^1 (1-t^2)^{\alpha-\frac{1}{2}} e^{-i x_d \lambda_d t} dt. \tag{3}$$

The function $\Psi_{\lambda,\alpha}$ has the following properties

i) $\Psi_{\lambda,\alpha}(x) = \Psi_{x,\alpha}(\lambda)$.

ii) for all $(x, \lambda) \in \mathbb{R}^d \times \mathbb{R}^d$ $|\Psi_{\lambda,\alpha}(x)| \leq 1$.

iii) it follows from Riemann-Lebesgue lemma that $\lim_{\lambda_d \to \infty} \Psi_{\lambda,\alpha}(x) = 0$.

2. HARMONIC ANALYSIS ASSOCIATED WITH $\Delta_{D,\alpha}$

Proposition 1 *$\Psi_{\lambda,\alpha}$ satisfies the differential equation*

$$\Delta_{d,\alpha} \Psi_{\lambda,\alpha} = -\|\lambda\|^2 \Psi_{\lambda,\alpha}.$$

Proof. Notice that $\Psi_{\lambda,\alpha}(x) = e^{-i\langle x', \lambda' \rangle} \displaystyle\int_0^1 (1-t^2)^{\alpha-\frac{1}{2}} e^{-i x_d, \lambda_d t} dt$, it's clear that

$$\Delta_{d,\alpha}(e^{-i\langle x', \lambda' \rangle}) = -\sum_{i=1}^{d-1} \lambda_i^2.$$

On the other hand we have

$$\Delta_{d,\alpha} \left(\int_0^1 (1-t^2)^{\alpha-\frac{1}{2}} e^{-i x_d \lambda_d t} dt \right) = -\lambda_d^2 \int_0^1 t^2 (1-t^2)^{\alpha-\frac{1}{2}} e^{-i x_d \lambda_d t} dt$$

$$- \quad i\frac{2\alpha+1}{x_d}\lambda_d \int_0^1 t(1-t^2)^{\alpha-\frac{1}{2}}(e^{-ix_d\lambda_d t}-1)dt,$$

but

$$\int_0^1 t(1-t^2)^{\alpha-\frac{1}{2}}(e^{-ix_d\lambda_d t}-1)dt = \frac{-i\lambda_d x_d}{2\alpha+1}\int_0^1 (1-t^2)^{\alpha+\frac{1}{2}}e^{-ix_d\lambda_d t}dt$$

it follows that

$$\begin{aligned}\Delta_{d,\alpha}\left(\int_0^1 (1-t^2)^{\alpha-\frac{1}{2}}e^{-ix_d\lambda_d t}dt\right) &= -\lambda_d^2\int_0^1\left(t^2(1-t^2)^{\alpha-\frac{1}{2}}+(1-t^2)^{\alpha+\frac{1}{2}}\right)\\ &\times\ e^{-ix_d\lambda_d t}dt\\ &= -\lambda_d^2\int_0^1(1-t^2)^{\alpha-\frac{1}{2}}e^{-ix_d\lambda_d t}dt.\end{aligned}$$

Hence $\Delta_{d,\alpha}\Psi_{\lambda,\alpha} = -\|\lambda\|^2\Psi_{\lambda,\alpha}$. ■

Definition 1 *The Weinstein type intertwining operator is the operator $\mathcal{R}_\alpha$ defined on $E(\mathbb{R}^d)$ by*

$$\mathcal{R}_\alpha f(x) = a_\alpha\int_0^1(1-t^2)^{\alpha-\frac{1}{2}}f(x',x_d t)dt. \tag{4}$$

Remark 1 *$\mathcal{R}_\alpha$ can be written in the following form*

$$\mathcal{R}_\alpha f(x) = a_\alpha sgn(x_d)|x_d|^{-2\alpha}\int_0^{x_d}(1-t^2)^{\alpha-\frac{1}{2}}f(x',t)dt,\ \ x_d\in\mathbb{R}^*.$$

Proposition 2 *For all $f\in E(\mathbb{R}^d)$ we have the following transmutation relation*

$$\Delta_{d,\alpha}(\mathcal{R}_\alpha f) = \mathcal{R}_\alpha(\Delta_d f),\ \ \textit{for all } f\in E(\mathbb{R}^d), \tag{5}$$

where Δ_d is the Laplacian on $\mathbb{R}^d$.

Proof. Notice that

$$\begin{aligned}\Delta_{d,\alpha}(\mathcal{R}_\alpha f)(x) &= \sum_{i=0}^{d-1}\frac{\partial^2\mathcal{R}_\alpha f(x',x_d)}{\partial x_d^2}+\frac{\partial^2\mathcal{R}_\alpha f(x',x_d)}{\partial x_d^2}\\ &+ \frac{2\alpha+1}{x_d}\left(\frac{\partial\mathcal{R}_\alpha f(x',x_d)}{\partial x_d}-\frac{\partial\mathcal{R}_\alpha f(x',0)}{\partial x_d}\right)\\ &= \sum_{i=0}^{d-1}\frac{\partial^2\mathcal{R}_\alpha f(x',x_d)}{\partial x_d^2}+\frac{\partial^2\mathcal{R}_\alpha f(x',x_d)}{\partial x_d^2}\\ &+ (2\alpha+1)\int_0^1\frac{\partial^2\mathcal{R}_\alpha f(x',tx_d)}{\partial x_d^2}dt.\end{aligned}$$

Since

$$\frac{\partial^2\mathcal{R}_\alpha(f)(x)}{\partial x_d^2} = a_\alpha\int_0^1(1-t^2)^{\alpha-\frac{1}{2}}t^2\frac{\partial^2\mathcal{R}_\alpha f(x',tx_d)}{\partial x_d^2}dt$$

it follows that

$$\Delta_{d,\alpha}(\mathcal{R}_\alpha(f)(x)) = a_\alpha\int_0^1(1-t^2)^{\alpha-\frac{1}{2}}t^2\frac{\partial^2\mathcal{R}_\alpha f(x',tx_d)}{\partial x_d^2}dt+J(x)$$

where

$$J(x) = (2\alpha+1)a_\alpha\int_0^1\int_0^1(1-s^2)^{\alpha-\frac{1}{2}}s^2\frac{\partial^2\mathcal{R}_\alpha f(x',stx_d)}{\partial x_d^2}dtds.$$

By Fubini's theorem

$$\begin{aligned} J(x) &= (2\alpha+1)a_\alpha \int_0^1 (1-s^2)^{\alpha-\frac{1}{2}} s \left(\int_0^s \frac{\partial^2 \mathcal{R}_\alpha f(x', tx_d)}{\partial x_d^2} dt \right) ds \\ &= (2\alpha+1)a_\alpha \int_0^1 \left(\int_t^1 (1-s^2)^{\alpha-\frac{1}{2}} s \right) ds \frac{\partial^2 \mathcal{R}_\alpha f(x', tx_d)}{\partial x_d^2} dt \\ &= a_\alpha \int_0^1 (1-t^2)^{\alpha+\frac{1}{2}} \frac{\partial^2 \mathcal{R}_\alpha f(x', tx_d)}{\partial x_d^2} dt \end{aligned}$$

hence

$$\begin{aligned} \Delta_{d,\alpha} \mathcal{R}_\alpha(f)(x) &= a_\alpha \int_0^1 (1-t^2)^{\alpha-\frac{1}{2}} \sum_{i=0}^{d-1} \frac{\partial^2 \mathcal{R}_\alpha f(x', tx_d)}{\partial x_d^2} dt \\ &+ a_\alpha \int_0^1 (1-t^2)^{\alpha-\frac{1}{2}} \frac{\partial^2 \mathcal{R}_\alpha f(x', tx_d)}{\partial x_d^2} dt \\ &= \mathcal{R}_\alpha(\Delta_d f)(x). \end{aligned}$$

Definition 2 *The dual of the Weinstein type intertwining operator $\mathcal{R}_\alpha$ is the operator ${}^t\mathcal{R}_\alpha$ defined on $D(\mathbb{R}^d)$ by*

$$ {}^t\mathcal{R}_\alpha(f)(y) = a_\alpha \int_{|y_d|}^\infty (s^2 - y_d^2)^{\alpha-\frac{1}{2}} f(y', sgn(y_d)s) s ds. \tag{6}$$

Proposition 3 *${}^t\mathcal{R}_\alpha$ satisfies for $f \in D(\mathbb{R}^d)$ and $g \in E(\mathbb{R}^d)$ the following relation*

$$\int_{\mathbb{R}^d} {}^t\mathcal{R}_\alpha(f)(y) g(y) dy = \int_{\mathbb{R}^d} f(y) \mathcal{R}_\alpha(g)(y) d\mu_\alpha(y). \tag{7}$$

Proof. Let $g \in E(\mathbb{R}^d)$ and $f \in D(\mathbb{R}^d)$, from Remarque 1 we have

$$\begin{aligned} \int_{\mathbb{R}^d} f(y) \mathcal{R}_\alpha(g)(y) d\mu_\alpha(y) &= \int_{\mathbb{R}^{d-1}} \int_0^\infty a_\alpha x_d^{-2\alpha} \left(\int_0^{x_d} (x_d^2 - t^2)^{\alpha-\frac{1}{2}} g(x', t) dt \right) \\ &\times f(x) |x_d|^{2\alpha+1} dx_d dx' \\ &- \int_{\mathbb{R}^{d-1}} \int_0^\infty a_\alpha x_d^{-2\alpha} \left(\int_{x_d}^0 (x_d^2 - t^2)^{\alpha-\frac{1}{2}} g(x', t) dt \right) \\ &\times f(x) |x_d|^{2\alpha+1} dx_d dx' \end{aligned}$$

the result follows directly from Fubini's theorem, a change of variable and the Chasles Formula. ■

Definition 3 *The Weinstein type transform $\mathcal{F}_{\alpha,d}$ is defined on $L^1_\alpha(\mathbb{R}^d)$ by*

$$\mathcal{F}_{\alpha,d}(f)(\lambda) = \int_{\mathbb{R}^d} f(x) \Psi_{\lambda,\alpha}(x) d\mu_\alpha(x), \text{ for all } \lambda \in \mathbb{R}^d. \tag{8}$$

Remark 2 *If f is an even function with the last variable then the Weinstein type transform $\mathcal{F}_{\alpha,d}$ coincides with the Weinstein transform $\mathcal{F}_\alpha$ defined by*

$$\mathcal{F}_\alpha(f)(\lambda) = \int_{\mathbb{R}^d_+} f(x) \Phi_{\lambda,\alpha}(x) x_d^{2\alpha+1} dx_d dx', \text{ for all } \lambda \in \mathbb{R}^d.$$

Proposition 4 *Let f and g in $L^1_\alpha(\mathbb{R}^d)$, we have*

$$\int_{\mathbb{R}^d} \mathcal{F}_{\alpha,d}(f)(x) g(x) d\mu_\alpha(x) = \int_{\mathbb{R}^d} f(x) \mathcal{F}_{\alpha,d}(g)(x) d\mu_\alpha(x).$$

Proof. As f and g in $L^1_\alpha(\mathbb{R}^d)$, it follows from (ii) and Fubini's theorem that

$$\begin{aligned}\int_{\mathbb{R}^d} |\mathcal{F}_{\alpha,d}(f)(x)g(x)|d\mu_\alpha(x) &= \int_{\mathbb{R}^d}\int_{\mathbb{R}^d} |f(\lambda)g(x)\Psi_{\lambda,\alpha}(x)|d\mu_\alpha(\lambda)d\mu_\alpha(x)\\ &\leq \|f\|_{L^1_\alpha(\mathbb{R}^d)}\|g\|_{L^1_\alpha(\mathbb{R}^d)}.\end{aligned}$$

From (iii) and Fubini's theorem we deduce the desired result. ■

Theorem 1 *(Plancherel theorem) For all $f \in S(\mathbb{R}^d)$ we have*

$$\int_{\mathbb{R}^d} |f(x)|^2 d\mu_\alpha(x) = C(\alpha)\left(\int_{\mathbb{R}^d} |\mathcal{F}_{\alpha,d}(f_e)(\lambda)|^2 d\mu_\alpha(\lambda) + \int_{\mathbb{R}^d} |\mathcal{F}_{\alpha,d}(|f_o|)(\lambda)|^2 d\mu_\alpha(\lambda)\right),$$

where $S(\mathbb{R}^d)$ is the Schwartz space of rapidly decreasing functions on $\mathbb{R}^d$ and $C(\alpha) = \dfrac{1}{(2\pi)^{\frac{d}{2}}2^\alpha\Gamma(\alpha+1)}$.

Proof. We have

$$\begin{aligned}\int_{\mathbb{R}^d} |f(x)|^2 d\mu_\alpha(x) &= \int_{\mathbb{R}^d} |f_e(x)+f_o(x)|^2 d\mu_\alpha(x)\\ &= \int_{\mathbb{R}^d} |f_e(x)|^2 d\mu_\alpha(x) + 2\int_{\mathbb{R}^d} f_e(x)f_o(x)d\mu_\alpha(x) + \int_{\mathbb{R}^d} |f_o(x)|^2 d\mu_\alpha(x),\end{aligned}$$

as $f_e f_o$ is an odd function respect to the last variable, it follows by Fubini's theorem that

$$\int_{\mathbb{R}^{d-1}}\int_{\mathbb{R}} f_e(x', x_d)f_o(x', x_d)|x_d|^{2\alpha+1}dx_d dx' = 0.$$

Since f_e and $|f_o|$ are even functions, then by Remarque 2 and Plancherel theorem for the Weinstein transform (see [5]) it follows that

$$\int_{\mathbb{R}^d} |f(x)|^2 d\mu_\alpha(x) = C(\alpha)\left(\int_{\mathbb{R}^d} |\mathcal{F}_{\alpha,d}(f_e)(\lambda)|^2 d\mu_\alpha(\lambda) + \int_{\mathbb{R}^d} |\mathcal{F}_{\alpha,d}(|f_o|)(\lambda)|^2 d\mu_\alpha(\lambda)\right).$$

Proposition 5

- *For all $f \in L^1_\alpha(\mathbb{R}^d)$, the function $\mathcal{F}_\alpha(f)$ is continuous on $\mathbb{R}^d$ and we have*

$$\|\mathcal{F}_{\alpha,d}(f)\|_{\alpha,\infty} \leq \|f\|_{\alpha,1}.$$

- *For all $f \in S(\mathbb{R}^d)$ we have*

$$\mathcal{F}_\alpha(f)(y) = \mathcal{F}_0 \circ^t \mathcal{R}_\alpha(f)(y), \quad \forall y \in \mathbb{R}^d$$

where $\mathcal{F}_0$ is the transformation defined by, for all $y \in \mathbb{R}^d$

$$\mathcal{F}_0(f)(y) = \int_{\mathbb{R}^d} f(x)e^{-i\langle y,x\rangle}dx, \quad \forall f \in D(\mathbb{R}^d).$$

Proof.

- Since $|\Psi_{\lambda,\alpha}(x)| \leq 1$, it follows that

$$|f(x)\Psi_{\lambda,\alpha}(x)| \leq |f(x)|.$$

As $\lim_{\lambda_d\to\infty} \Psi_{\lambda,\alpha}(x) = 0$, it follows from the dominated convergence theorem that

$$\|\mathcal{F}_{W,\alpha}(f)\|_{\alpha,\infty} \leq \|f\|_{\alpha,1}.$$

•

$$\begin{aligned}\mathcal{F}_0 \circ^t \mathcal{R}_\alpha(f)(y) &= a_\alpha \int_{\mathbb{R}^{d-1}} e^{-i\langle x',y'\rangle} \int_0^\infty \int_{x_d}^\infty (s^2-x_d^2)^{\alpha-\frac{1}{2}} x_d f(x',s) dx_d e^{-ix_d y_d} ds dx' \\ &+ a_\alpha \int_{\mathbb{R}^{d-1}} e^{-i\langle x',y'\rangle} \int_0^\infty \int_{x_d}^\infty (s^2-x_d^2)^{\alpha-\frac{1}{2}} x_d f(x',-s) dx_d e^{ix_d y_d} ds dx'\end{aligned}$$

From Fubini's theorem, we obtain

$$\begin{aligned}\mathcal{F}_0 \circ^t \mathcal{R}_\alpha(f)(y) &= a_\alpha \int_{\mathbb{R}^{d-1}} e^{-i\langle x',y'\rangle} \int_0^\infty \int_0^{x_d} (s^2-x_d^2)^{\alpha-\frac{1}{2}} x_d f(x',s) dx_d e^{-ix_d y_d} ds dx' \\ &+ a_\alpha \int_{\mathbb{R}^{d-1}} e^{-i\langle x',y'\rangle} \int_0^\infty \int_0^{x_d} (s^2-x_d^2)^{\alpha-\frac{1}{2}} x_d f(x',-s) dx_d e^{ix_d y_d} ds dx'.\end{aligned}$$

By a change of variable and using relation (3), we find that

$$\begin{aligned}\mathcal{F}_0 \circ^t \mathcal{R}_\alpha(f)(y) &= \int_{\mathbb{R}^{d-1}} \left(\int_0^\infty f(x) \Psi_{\lambda,\alpha}(x) |x_d|^{2\alpha+1} dx_d dx' \right) \\ &+ \int_{\mathbb{R}^{d-1}} \left(\int_0^\infty f(x) \Psi_{\lambda,\alpha}(x) |x_d|^{2\alpha+1} dx_d dx' \right)\end{aligned}$$

$$\mathcal{F}_0 \circ^t \mathcal{R}_\alpha(f)(y) = \int_{\mathbb{R}^{d-1}} \int_{-\infty}^\infty f(x) \Psi_{\lambda,\alpha}(x) |x_d|^{2\alpha+1} dx_d dx' = \mathcal{F}_{\alpha,d}(f)(y).$$

3. APPLICATION

In this section we will give an application about Annihilating sets.

Definition 4 *Let S, Σ be two measurable subsets of $\mathbb{R}^d$. Then (S,Σ) is called a weak annihilating pair for the Weinstein type transform if supp$f \subset S$ and supp$\mathcal{F}_\alpha(f) \subset \Sigma$ implies that $f = 0$, where supp $f = \{x : f(x) \neq 0\}$.*

Definition 5 *Let S, Σ be two measurable subsets of $\mathbb{R}^d$. Then (S,Σ) is called a strong annihilating pair for the Weinstein type transform if there exists a constant $C(S,\Sigma)$ such that for all function $f \in L^2(\mathbb{R}^d, \mu_\alpha)$, with supp $\mathcal{F}_\alpha(f) \subset \Sigma$,*

$$\|f\|_{L^2(\mathbb{R}^d_+,\mu_\alpha)} \leq C(S,\Sigma) \|f\|_{L^2(S^c,\mu_\alpha)} \tag{9}$$

where $\mu_\alpha(x) = |x_d|^{2\alpha+1} dx' dx_\alpha$ and $S^c = \mathbb{R}^d_+ \backslash S$.

Theorem 2 *Let S and Σ be a pair of measurable subsets of $\mathbb{R}^d$ with $0 < \mu_\alpha(S)$, $\mu_\alpha(\Sigma) < \infty$, then the pair (S,Σ) is strong annihilating pair.*

Proof. The proof is similar to that of Theorem B in [7]. ■

REFERENCES

[1] Ben Nahia, Z, Ben Salem, N: Spherical harmonics and applications associated with the Weinstein operator. In: Potential Theory - ICPT 94, vol. 94, pp. 233-242 (1996)

[2] Ben Nahia, Z, Ben Salem, N: On a mean value property associated with the Weinstein operator. In:Potential Theory - ICPT 94, vol. 94, pp. 243-254 (1996)

[3] Brelot, M: Equation de Weinstein et potentiels de Marcel Riesz. In: Sminaire de Thorie du Potentiel, No.3 (Paris, 1976/1977). Lecture Notes in Math., vol. 681, pp. 18-38 (1978)

[4] Chettaoui, C, Trimche, K: Bockner-Hecke theorems for the Weinstein transform and applications. Fract.Calc. Appl. Anal. 13(3), 261-280 (2010)

[5] Mejjaoli, H, Salhi, M: Uncertainty principles associated with the Weinstein transform. Czechoslov. Math.J. 61(4), 941-974 (2011)

[6] Othmani, Y, Trimche, K: Real Paley-Wiener theorems associated with the Weinstein operator. Mediterr.J. Math. 3(1), 105-118 (2006)
*[7] Pillipe Jaming, Saifallah Ghobber, Uncertainty principles for integral operators. Studia Mathematica,INSTYTUT MATEMATYCZNY * POLSKA AKADEMIA NAUK, 2014, 220, pp.197-220.*

Review on Lithium-Ion battery modeling for different applications

Jaouad Khalfi1, Najib Boumaaz1, Abdallah Soulmani1

1Department of Physics, Laboratory of Electrical Systems, Energy Efficiency and Telecommunications, Faculty of Sciences and Technology, Cadi Ayyad University, Marrakech, Morocco Technology, J&K, India.

ABSTRACT

Battery modeling is one of the most important functions in a battery management system for different applications such as electrical vehicles, This article focuses on state of the art of lithium-ion battery modeling by exploring different existing modeling methods, such as Electrochemical models, Analytical models and the equivalent electrical circuit. First, the characteristics of the lithium-ion battery for different applications are reviewed ,we chose to study this type of battery because it offers satisfactory characteristics compared to other battery types, then the different modeling methods have been explored, finaly a conclusion with suggestion of other modeling type such as fractional order model have been proposed to improve efficiency and precision of battery management system.

Keywords: Battery modeling ,Lithium-ion battery, Electrochemical models, Analytical models , Equivalent electrical circuit model, Fractional order model

1. INTRODUCTION

Today, there are many applications for energy storage systems. The batteries are the most famous.
They are used in several industries, such as electric and hybrid vehicles, renewable energy systems and marine energy systems. Batteries are used as back-up in wind or photovoltaic energy conversion systems. They are implemented to store excess energy captured by wind power or sunlight using wind turbines in windy or sunny weather, as well as to release stored energy during stationary periods or during the night. In electric or hybrid trains and vehicles, a battery is used to store energy from the regenerative braking system and to return energy to the system when the train is in traction mode. They can increase the reliability of hybrid systems.
Different chemical batteries are widely used in these applications as: lead-acid, nickel cadmium (NiCd), nickel-metal hydride (NiMH) and lithium ion (Li-ion), Compared with other battery systems, Li-Ion battery offers many advantages such as lightness, high energy density and ease of manufacture, they also have excellent energy density, do not have memory effect and have a long lifespan. [1-6] The electrochemical behavior of the accumulator is at the origin of the two main sources of heat to which it is subjected. The Joule effect, called irreversible, results from the electrical nature of the battery, while the reversible heat comes from chemical reactions at the level of the electrodes. Optimizing a Li-Ion battery model for a given application necessarily involves saving a large amount of time and experimental effort, thus saving considerable time and money as well as having a good battery.
Precise modeling and simulation of this type of battery is necessary in order to examine its performance and different modeling approaches exist: electrical modeling, "black box" modeling, energy modeling, physicochemical modeling.
Modeling of electrical circuits is a useful model presented by many researchers. In the modeling of the electrical circuit, the electrical characteristics of the battery are taken into account and passive linear elements are used. Such models are presented in different papers [7-12].

"Black box" modeling connects the possible system responses to a specific type of stimuli, regardless of the mechanisms responsible for its behavior. The accumulator is represented by a black box with inputs and outputs that consist of physical quantities related to the operation and conditions of use. In general, inputs are composed of current, state of charge, temperature, and state of aging when it is possible to estimate it. The magnitude that we want to estimate at the output is generally the tension. The box consists of an estimator that is able to predict the values of the outputs according to the inputs. Examples of estimators are presented in [13-15].

Energy modeling models all energy flows within the electrochemical battery without the use of partial differential equations. It consists of processing energy flows of different types: electrical, thermal, or fluidic.

Physicochemical modeling is seldom used in the domain of electrical engineering. It uses the principles of chemistry and physics to describe the precise behavior of the battery cell. Its main interest is that it facilitates the understanding of the phenomena that limit the performance of the cells, and the fundamental mechanisms of the generation of the power, making it possible to further improve the batteries' construction processes and design. These models require accurate and functional knowledge of many parameters (electrolyte concentration, diffusion coefficient, transfer coefficient, and electrode geometry). In [16-17], the authors present some electrochemical models for lithium-ion batteries.

In this paper, we present different types of modeling suitable for estimating the condition of a lithiumion battery in the context of its use in battery management systems for different applications such as electric vehicles. These are electronic devices that include, among other things, computers on which we want to implement the observer. Their computing power and memory are very limited, which is why the model used must be numerically efficient and sober. After a general introduction in the first part. In the second part, we do a bibliographical review of electrochemical accumulators such as lithium-ion batteries available in the literature. In the third part, we present the different types of lithium-ion battery modeling, namely electrochemical models (such as Particle models (PM) and Porous electrode Model), then analytical models (such as Kinetic battery model) and finally models based on equivalent electrical circuits (such as First order model and multiple order model). And the last part is devoted to a conclusion that sums up all the work done in this article.

2. ELECTROCHEMICAL ACCUMULATOR

An electrochemical generator is a source of electrical energy obtained through the direct transformation of chemical energy. Three main categories of electrochemical generators exist, namely: batteries, accumulators and fuel cells. The history of electrochemical generators begins in 1800 with Alessandro Volta, who invented the non-rechargeable primary cell. This stack is formed by a stack of alternating copper and zinc disks. In alternations, there are separating washers soaked in brine (H_2O + NaCl) which allow the conduction of the current. This process makes it possible to obtain a generator formed of a zinc anode and a copper cathode, the whole being bathed in an electrolyte (brine) thus ensuring the movement of the electrons. However, Volta's battery is not rechargeable. The photo of a voltaic pile can be found in Figure 1.

Later in 1859, Gaston Planté, discovering the reversibility of electrical chemical reactions thanks to the reversal of the direction of the current, invented the lead accumulator. It is composed of lead alloy grids pasted with a mixture of sulfuric acid, lead oxide and water which constitutes the active ingredient. In 1899, this technology enabled an electric car in the shape of a torpedo to travel 100 km / h [18]. It was the first type of rechargeable battery marketed. Lead-acid batteries are still used in vehicles today for 12V and 15V power supplies. The success of this type of battery is due to the low cost of lead and sulfuric acid, their ease of manufacture and their lifespan of a few years [19]. The photo of a lead accumulator

can be found in Figure 1.

Nickel-Cadmium (Ni - Cd) batteries have replaced lead batteries because they are more robust and powerful. In 1899, these accumulators were used for the electric vehicle "Jungner" and in 1900 for "Edison".

However, the high cost and the very high toxicity limit the use of this type of accumulator [19].

Marketed in 1990, Nickel-Metal-Hydride (Ni –MH) batteries make it possible to overcome the toxicity of cadmium and have energy densities 30% higher than those of Ni-Cd batteries. In addition, these batteries operate at low temperature and have a low manufacturing cost. However, the use of these batteries has been reduced since the advent of accumulators based on lithium. Indeed, Ni –MH batteries have very moderate specific energy densities, which do not meet the criteria for reducing the weight of accumulators imposed by on-board applications.

(a) The Voltaic battery (b) Gaston Planté's battery.

Figure 1. Electrochemical generators

In 1991, the first rechargeable batteries based on lithium were marketed by the Japanese manufacturer Sony [20]. This technology quickly becomes predominant because of its performance in terms of specific energy, load capacity and electromotive force (emf). Table 1 summarizes these various battery technologies with their characteristics.

Table 1. Comparative table of the various battery technologies.

Type	EMF	Number of cycles	Charging Efficiency (%)	Massic Energy (Wh/kg)	volume energy density (Wh/l)	T (°C)
lead-acid	2, 1	500 to 1200	–	15 to 45	40 – 80	−40 to 40
Nickel-Cadmium	1, 2	≈ 2000	60	30 to 60	80	−20 to 60
nickel metal hydride	1, 2	500 to 1200	60	100	200	−20 to 60
Lithium-Polymer	3, 7	≈ 1000	–	100 to 130	140 – 435	−40 to 40
Lithium-ion	3, 6	1000 to 10000	95	150	300	−20 to 60

2.2.The Li-ion cell

The Li-ion battery is based on the reversible exchange of Li+ ion between the anode and the cathode. The anode and the cathode are separated by a material that allows lithium ions to pass through but not electrons: the separator. The separator can be a polymer film (polyethylene, polypropylene) or a microporous ceramic [19].

Nowadays, the anode is graphite and the cathode is often formed from lithiated transition metal oxide such as cobalt dioxide (CoO2) or manganese (MnO2). The electrolyte is often non-aqueous: a lithium salt in an organic solvent [21]. Figure 2 illustrates the operation of a Li-ion cell in discharge. The e−electrons travel from the anode to the cathode through the outer circuit. The presence of negative charges (electrons) in the cathode attracts Li +ions which pass from the anode to the cathode through the separator to collect the missing charges. When all of the cycling lithium passes through the cathode, the battery is discharged. The reverse phenomenon occurs during charging and allows lithium to return to the anode. Equations 1 (respectively 2) represent the electrochemical reactions taking place in the cathode (respectively anode) when using the Li-Ion cell. The variable "M" represents the metal used at the cathode.

At the positive electrode (cathode) we have:

$$Li_{y-z}MO_2 + zLi^+ + z\,e^- \leftrightarrows LiyMO_2 \qquad (1)$$

At the negative electrode (anode) we have:

$$Li_xC_6 \leftrightarrows Li_{x-z}C_6 + zLi^+ + z\,e^- \qquad (2)$$

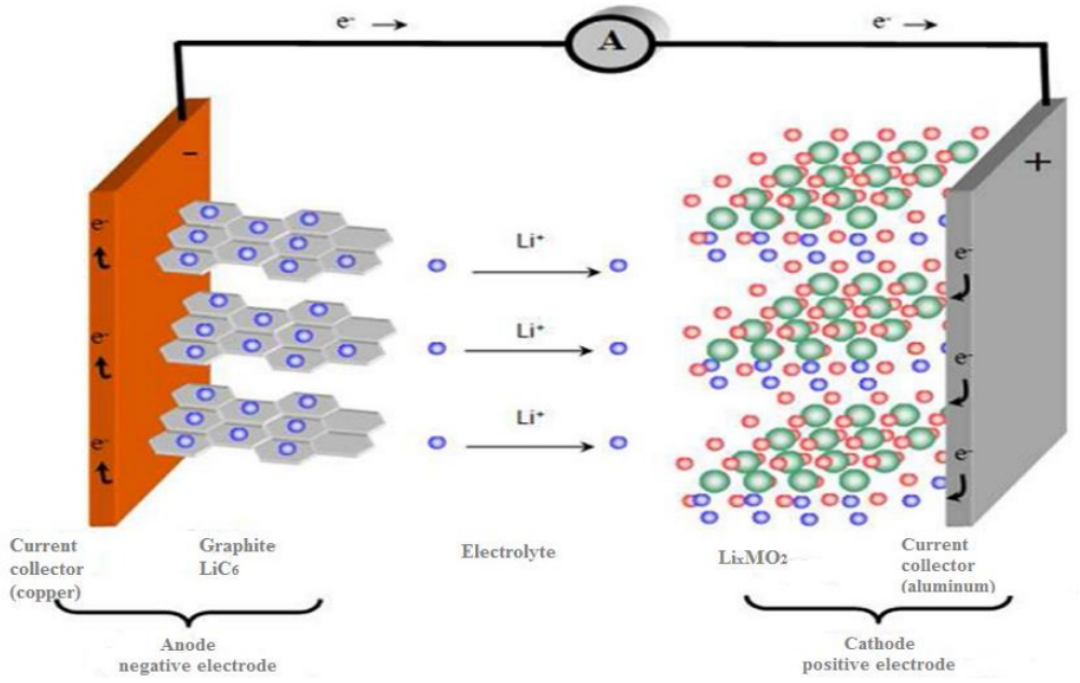

Figure 2. Structure of a Li-ion battery during a discharge

Lithium-ion batteries have attracted attention compared with other types of batteries since they have several advantages, high power density, high energy density, strong environmental adaptability, 'long life, and high cell voltage. However, there are several types of lithium-ion batteries, each type has its own advantages, such as LMOq which has a high specific power, LCO, which has a high specific

energy, lithium-ion batteries NCA and NMC, which are the most thermally stable and cheapest, LTO, which has fast charging, long life and but higher cost and low specific energy [22]. Table 2 shows commercial lithium-ion batteries and their different characteristics.

Table 2. Comparison between commercial batteries of lithium-ion [23].

Abbrev.	LCO	LNO	LMO	NMC	LFP	NCA	LTO
Battery Name	Lithium cobalt oxide	Lithium nickel oxide	Lithium manganese oxide	Lithium nickel manganese	Lithium iron phosphate	Lithium nickel cobalt aluminum oxide	Lithium titanate
Year	since 1991	since 1996	since 1996	since 2008	since 1993	since 1999	since 2008
Nominal Tension (V)	3.7~3.9	3.6~3.7	3.7~4.0	3.8~4.0	3.2~3.3	3.6~3.65	2.3~2.5
Specific Energy (Wh/kg)	150~200	150~200	100~150	150~220	90~130	200~260	70~85
Charge (C)	0.7~1	0.7~1	0.7~1	0.7~1	1	0.7	1
Discharge (C)	1	1	1	1	1	1	10
Lifespan	500~1000	>300	300~700	1000~2000	1000~2000	500	3000~7000
Thermal Runaway (C)	150	150	250	210	270	150	-

3. LITHIUM BATTERY MODELING

3.1. Electrochemical models

Electrochemical models are the most sophisticated and rely on the kinetics of chemical reactions and transport equations [24]. They can to simulate the characteristics and reactions of a cell even before it is manufactured. The Pseudo-two-dimensional (P2D) model and the single particle model are among the most popular in this category [25]. According to paper [25], a battery management system (BMS) which would be based on an electrochemical model would have significant advantages over those based on empirical models.

Particle models (PM) : The electrochemical particle model is based on two principles. First, each electrode is modeled as a spherical particle within which the intercalation and deintercalation processes occur. In this model, variations in the potential or concentration of the electrolyte are ignored. The single particle

model (SPM), Figure 3.a) has a much faster response than the porous electrode model (PEM), but fails to represent high current discharges [25]. The Multiple Particle Model (MPM), Fig. 3.b) has been proposed to take into account the size and varying conduction resistance of cathode oxide particles, mainly for LiFePo4 batteries [26-28].

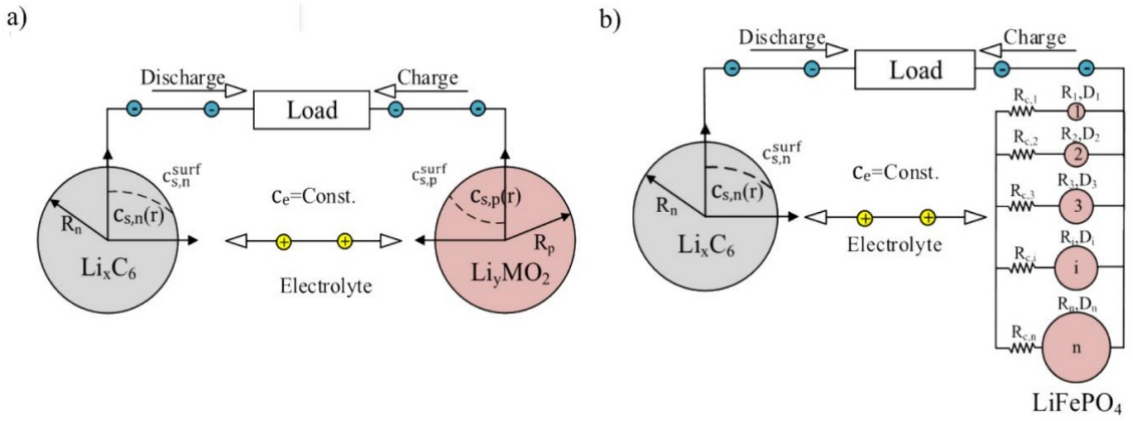

Figure 3 - Particle model: a) single, b) multiple [25]

Porous electrode Model : The PEM (Figure 4), is an evolution of the SPM taking into account the variation of the potential and the concentration. The PEM is based on kinetic equations, solution concentration theories and porous electrode theory [25, 29, 30]. This model is mainly used to study the local current density inside lithium-ion cells [31] with results close to experimental [32]. It captures the dynamics of lithium diffusion and the kinetics of charge transfer. It is a rigorous and precise model, but far too heavy for the computational capacities of an on-board system [33].

The physical models can be theoretical, analytical or electrochemical. In-depth knowledge of the materials and internal properties of cell construction, rarely provided by battery manufacturers, is required in the construction of these models. They are complex and difficult to implement.

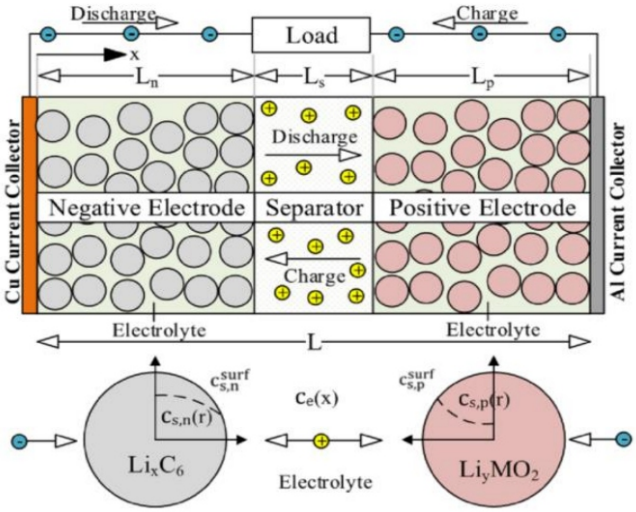

Figure 4. Porous electrode Model (PEM) [25]

3.2. Analytical models

The representation of the nonlinear kinetics of batteries by differential equation was the subject of research in the early of 1990s by Manwell and McGowan [34-35]. This model is better known as the Kinetec Battery Model (KiBaM). It is called kinetics because it uses the principles of the kinetics of chemical reactions as a basis. In this model based on a hydraulic analogy, the loads are distributed in two reservoirs: the reservoir of available loads y1 and that of limited loads y2 (fig.5). The current delivered i (t) by the battery corresponds to the liquid flow rate at the outlet.

Rakhmatov and Vrudhula [36] have developed a model based on the diffusion of lithium ions in the electrolyte which predicts the autonomy of a battery. Jongerden and Haverkot [37] denote similarities between the scattering model and the kinetic model, proving that the former was in fact the continuous representation of the latter. Analytical models cannot estimate voltage drop, aging, or heat generation. This makes this type of model unsuitable for use for any reason other than estimating the capacity of a battery. However, the hydraulic analogy is an interesting representation for understanding concepts and teaching battery science.

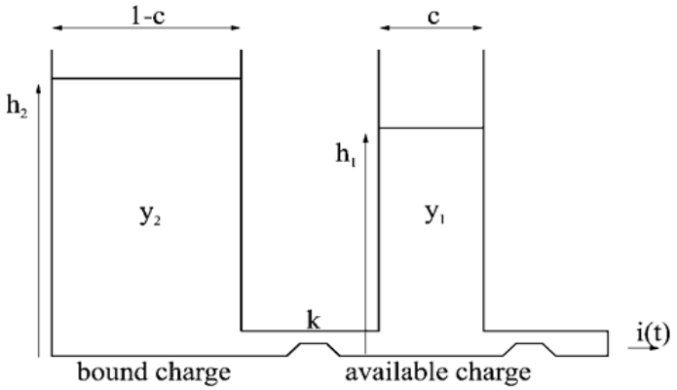

Figure 5. Kinetic battery model (KiBaM) [37]

3.3. The equivalent electrical circuit

The idea here is to represent the accumulator using an electrical circuit which takes its physical parameters into account. The classic approach to representing a voltage source is by an electromotive force in series with an ohmic resistance: U = E - RI. This simple approach makes it possible to quickly obtain an approximation of the behavior of the cell. You can add one or more R // C circuits depending on the precision you want to achieve.

First order model: This is a simple model which highlights the ohmic resistance (R0) of the cell as well as the phenomenon of diffusion (RD, CD). The variable Vt represents the terminal voltage of the cell, VD the voltage across the resistor RD in parallel with the capacitor CD, and OCV represents the no-load voltage of the cell.

$$\begin{cases} \frac{dV_D}{dt} = \frac{-V_D}{R_D C_D} + \frac{I}{C_D} \\ V_t = OCV - IR_0 - V_D \end{cases} \quad (3)$$

Multiple order model: This is the generalization of the first order model to a number n ≥ 2 of R // C circuits as illustrated in figure 6 and equation 4 for 1 ≤ i ≤ n. This approach increases the accuracy of the state of charge estimate because the low frequency behavior of the battery is better represented. But, this comes at the cost of greater model complexity.

$$\begin{cases} \frac{dV_{Di}}{dt} = \frac{-V_{Di}}{R_{Di} C_{Di}} + \frac{I}{C_{Di}} \\ V_t = OCV - IR_0 - \sum_{i=1}^{n} V_{Di} \end{cases} \quad (4)$$

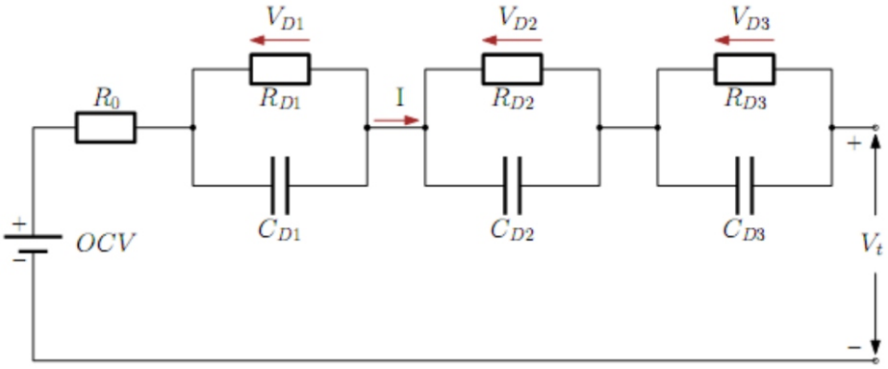

Figure 6. EEC model: Equivalent electrical circuit of order 3 [38]. OCV is the no-load voltage at rest (relaxed state) of the battery.

Consideration of hysteresis: Apart from the scattering which can to a certain extent be modeled by R // C branches, the Li-ion cell exhibits another non-linear behavior which is hysteresis. Indeed, when we observe the curve (f (SoC) = OCV) of the no-load voltage as a function of the state of charge of a Li-ion cell, we notice that the curves in charge and in discharge are different. This behavior of the Li-ion cell corresponds to a hysteresis phenomenon. Although very weak, this phenomenon still exists. Often in the literature, an average of the two curves is used to obtain a single representation of the relation f (SoC) = OCV. Sometimes, for more precision we find models allowing to better model this phenomenon. A distinction is made between the 0-state hysteresis model and the 1-state hysteresis model.

0-state hysteresis model: This is the simplest model, adding a term to the voltage measurement equation [39]. This term takes into account the fact that the hysteresis does not change sign directly with current. The system takes a long time to switch from one major hysteresis loop to another. The state equation of the system is given by:

$$\begin{cases} \mathrm{SoC_{k+1}} = \mathrm{SoC_k} - \left(\frac{\mathrm{n_i T_e}}{600\mathrm{Q_n}}\right)\mathrm{I_k} \\ \mathrm{V_t} = \mathrm{OCV} - \mathrm{I_k R_0} - \mathrm{s_k M_0(SoC_k)} \end{cases} \qquad (5)$$

where Te is the sampling period, SoCk is the state of charge at instant k × Te, sk the sign of the current flowing through the cell and M0 (SoCk) is half of the difference between the curves f (SoC) = OCV charging and discharging depending on the state of charge SoCk and Qn the charging capacity of the cell in Ah.

4. CONCLUSION

In this paper, our aim was to explore the different modeling types of lithium-ion battery, we focused on lithium-ion battery due to its many advantages such as lightness, high energy density and ease of manufacture.

The literature offers a wide variety of lithium-ion battery models. It is often presented as being made up of three families. The first family is formed by physical models which describe batteries as electrochemical objects, since the main phenomena at work relate to electrochemistry. These models have the advantage of being precise but are generally more complex and heavier in term of power calculation. A second family includes Analytical models. And the last family includes the models which describe the electrical behavior of the battery, which are the equivalent electric models.

Considering the other different approaches in the literature, we can suggest fractional order model is a mathematical representation that is justified for two main reasons:

- It allows the physical behavior of the cell to be well modeled because the same types of transfers are obtained using simplified electrochemical models.
- It is more precise than the other models' types, with an equivalent computational complexity.

REFERENCES

[1] Lai X, Gao W, Zheng Y et al (2019) A comparative study of global optimization methods for parameter identifcation of different equivalent circuit models for Li-ion batteries. Electrochim Acta 295:1057–1066 2.

[2] Song Z, Hofmann H, Lin X et al (2018) Parameter identifcation of lithium-ion battery pack for diferent applications based on Cramer-Rao bound analysis and experimental study. Appl Energy 231:1307–1318

[3] Ali E (2014) Advanced electric drive vehicles. CRC Press, Boca Roton 4.

[4] Chemali E, Preindl M, Malysz P et al (2016) Electrochemical and electrostatic energy storage and management systems for electric drive vehicles: State-of-the-art review and future trends. IEEE J Emerg Select Topics in Power Electron 4(3):1117–1134 5.

[5] Lu L, Han X, Li J et al (2013) A review on the key issues for lithium-ion battery management in electric vehicles. J Power Sources 226:272–288

[6] Dedryvere R, Foix D, Franger S et al (2010) Electrode/electrolyte interface reactivity in high-voltage spinel LiMn1. 6Ni0. 4O4/Li4Ti5O12 lithium-ion battery. J Phys Chem C 114(24):10999–11008

[7] TRAN, Manh-Kien, MEVAWALA, Anosh, PANCHAL, Satyam, et al. Effect of integrating the hysteresis component to the equivalent circuit model of Lithium-ion battery for dynamic and non-dynamic applications. Journal of Energy Storage, 2020, vol. 32, p. 101785.

[8] BACCOUCHE, Ines, MANAI, Bilal, et AMARA, Najoua Essoukri Ben. SoC estimation of LFP Battery Based on EKF Observer and a Full Polynomial Parameters-Model. In: 2020 IEEE 91st Vehicular Technology Conference (VTC2020-Spring). IEEE, 2020. p. 1-5.

[9] S. Panchal, I. Dincer, M. Agelin-Chaab, M. Fowler, and R. Fraser, "Uneven temperature and voltage distributions due to rapid discharge rates and different boundary conditions for series-connected LiFePO 4 batteries," Int. Commun. Heat Mass Transf., vol. 81, pp. 210–217, Feb. 2017.

[10] S. Panchal et al., "Cycling degradation testing and analysis of a LiFePO 4 battery at actual conditions," Int. J. Energy Res., vol. 41, no. 15, pp. 2565–2575, Dec. 2017.

[11] B. Xia et al., "Online Parameter Identification and State of Charge Estimation of Lithium-Ion Batteries Based on Forgetting Factor Recursive Least Squares and Nonlinear Kalman Filter," Energies, vol. 11, no. 1, p. 3, Dec. 2017.

[12] Z. Li, R. Xiong, and H. He, "An Improved Battery On-line Parameter Identification and State-of-charge Determining Method," Energy Procedia, vol. 103, pp. 381–386, Dec. 2016.

[13] ZAZI, Malika, et al. Nonlinear black box modeling of a lead acid battery using Hammerstein-Wiener model. Journal of Theoretical and Applied Information Technology, 2016, vol. 89, no 2, p. 476.

[14] HOW, Dickshon NT, HANNAN, Mahammad A., LIPU, Molla S. Hossain, et al. State-of-charge estimation of Liion battery in electric vehicles: A deep neural network approach. IEEE Transactions on Industry Applications, 2020, vol. 56, no 5, p. 5565-5574.

[15] E. M. Laadissi, A. E. Filali, and M. Zazi, "A Nonlinear TSNN Based Model of a Lead Acid Battery," Bulletin of Electrical Engineering and Informatics, vol. 7, no. 2, p. 169-175, 2018.

[16] LI, Weihan, FAN, Yue, RINGBECK, Florian, et al. Electrochemical model-based state estimation for lithium-ion batteries with adaptive unscented Kalman filter. Journal of Power Sources, 2020, vol. 476, p. 228534

[17] LI, Weihan, CAO, Decheng, JÖST, Dominik, et al. Parameter sensitivity analysis of

of electrochemical model-based battery management systems for lithium-ion batteries. Applied Energy, 2020, vol. 269, p. 115104.
[18] URBAIN, Matthieu. Modélisation électrique et énergétique des accumulateurs Li-Ion. Estimation en ligne de la SOC et de la SOH. 2009. Thèse de doctorat. Institut National Polytechnique de Lorraine
[19] Miomandre, F., Sadki, S., Audebert, P., and Méallet-Renault, R. (2011). Électrochimie - 2e éd. : Des concepts aux applications. Dunod. GoogleBooks-ID: zis0_5G_x4Sc
[20] EDDAHECH, Akram. Modélisation du vieillissement et détermination de l'état de santé de batteries lithium-ion pour application véhicule électrique et hybride. 2013. Thèse de doctorat.
[21] MAYÉ, Pierre. Générateurs électrochimiques : Piles, accumulateurs et piles à combustible. Dunod, 2010
[22] Ianniciello, L.; Biwolé, P.H.; Achard, P. Electric vehicles batteries thermal management systems employing phase change materials. J. Power Sources 2018, 378, 383–403.
[23] Wang, Q.; Jiang, B.; Li, B.; Yan, Y. A critical review of thermal management models and solutions of lithium-ion batteries for the development of pure electric vehicles. Renew. Sustain. Energy Rev. 2016, 64,106–128.
[24] M. Jongerden and B. Haverkort, "Which battery model to use?," Software, IET, vol. 3,pp. 445–457, Dec. 2009
[25] A. Jokar, B. Rajabloo, M. Désilets, and M. Lacroix, "An inverse method for estimating the electrochemical parameters of lithium-ion batteries: I. methodology," Journal of The Electrochemical Society, vol. 163, no. 14, pp. A2876–A2886, 2016.
[26] M. Safari and C. Delacourt, "Simulation-based analysis of aging phenomena in a commercial graphite/lifepo4 cell," Journal of The Electrochemical Society, vol. 158, no. 12, pp. A1436–A1447, 2011.
[27] M. Farkhondeh and C. Delacourt, "Mathematical modeling of commercial lifepo4 electrodes based on variable solidstate diffusivity," Journal of The Electrochemical Society, vol. 159, no. 2, pp. A177–A192, 2011.
[28] M. Farkhondeh, M. Safari, M. Pritzker, M. Fowler, T. Han, J. Wang, and C. Delacourt, "Full-range simulation of a commercial lifepo4 electrode accounting for bulk and surface effects: A comparative analysis," Journal of The Electrochemical Society, vol. 161, no. 3, pp. A201–A212, 2014.
[29] J. Newman and W. Tiedemann, "Potential and current distribution in electrochemical cells: Interpretation of the half cell voltage measurements as a function of reference-electrode location," Journal of The Electrochemical Society, vol. 140, no. 7, pp. 1961–1968, 1993.
[30] M. Doyle and J. Newman, "The use of mathematical modeling in the design of lithium/polymer battery systems," Electrochimica Acta, vol. 40, no. 13-14, pp. 2191–2196,1995. International symposium on polymer electrolytes.
[31] K. Lee, G. Kim, and K. Smith, "3d thermal and electrochemical model for spirally wound large format lithium-ion batteries (presentation)," tech. rep., National Renewable Energy Laboratory (NREL), Golden, CO., 2010.
[32] M. Doyle, J. Newman, A. S. Gozdz, C. N. Schmutz, and J.-M. Tarascon, "Comparison of modeling predictions with experimental data from plastic lithium-ion cells," Journal of The Electrochemical Society, vol. 143, no. 6, pp. 1890–1903, 1996.
[33] A. Jokar, B. Rajabloo, M. Désilets, and M. Lacroix, "An inverse method for estimating the electrochemical parameters of lithium-ion batteries: I. methodology," Journal of The Electrochemical Society, vol. 163, no. 14, pp. A2876–A2886, 2016.
[34] J. Manwell and J. McGowan, ""lead acid battery storage model for hybrid energy systems,"Solar Energy, vol. 50, pp. 399–405, 1993.

[35] J. M. et al., "Evaluation of battery models for wind/hybrid power system simulation," in in Proceedings of the 5th European Wind Energy Association Conference (EWEC '94), pp. 1182–1187, 1994.

[36] D. Rakhmatov and S. Vrudhula, "An analytical high-level battery model for use in energy management of portable electronic systems," in Proc. 2001 IEEE/ACM Int'l Conf. Computer-Aided Design (I. Press, ed.), pp. 488–493, 2001.

[37] M. Jongerden and B. Haverkort, "Which battery model to use ?," Software, IET, vol. 3, pp. 445–457, Dec. 2009.

[38] Lin, C., Mu, H., Xiong, R., and Shen, W. (2016). A novel multi-model probability battery state of charge estimation approach for electric vehicles using Hinfinity algorithm. Applied Energy, 166(Supplement C) :76–83.

[39] Plett, G. L. (2004b). Extended Kalman filtering for battery management systems of LiPB-based HEV battery packs: Part 2. Modeling and identification. Journal of Power Sources, 134(2): 262–276

Titchmarsh Theorems and K-Functionals for the Two-Sided Quaternion Fourier Transform

Azzedine Achak1, Radouan Daher2, Najat Safouane3

1Ecole Suprieure d'Education et Formation. Universit Chouaib Doukkali, El Jadida Morocco

2,3Department of Mathematics, Faculty of Sciences An Chock. University of Hassan II Casablanca 20100, Morocco

A B S T R A C T

The purpose of this paper is to study the Quaternion Fourier transforms of functions that satisfy Lipschitz conditions of certain orders. Thus we study the Quaternion Fourier transforms of Lipschitz function in the functions space Lr ®2, H), where Ha quaternion algebra which will be specified in due course. Our investigation into the problem was motivated by a theorem proved by Titchmarsh [[29], Theorem 85] for Lipschitz functions on the real line. we will give also some results on calculation of the K-functional which have number of applications of interpolation theory. In particular some recent problems in image processing and singular integral operators require the computation of suitable K-functionals. In this paper we will give some results con cerning the equivalence of a K-functional and the modulus of smoothness constructed by the Steklov function.

Keywords: Quaternion Fourier transform, Lipschitz class, Dini-Lipschitz class, Titchmarsh theorem, K-functional

1. INTRODUCTION

The quaternionic Fourier transform (QFT) plays a vital role in the representation of signals. It transforms a real (or quaternionic) 2D signal into a quaternion-valued frequency domain signal. The four QFT components separate four cases of symmetry in real signals instead of only two in the complex FT [8, 16]. In addition, understanding the QFT paves the way for understanding other integral transform, such as the Quater nion Fractional Fourier transform (QFRFT) [10, 23, 31, 17, 18], Quaternion linear canonical transform (QLCT) [24] and Quaternion Wigner-Ville distribution [6]. Due to the non-commutativity of multiplication of quaternions, there are different types of QFTs and we focus on the right-sided QFT (RQFT) and two-sided QFT (SQFT).

Recently it has become popular to generalize the Fourier transform (FT) from real and complex numbers [7] to quaternion algebra. In these constructions many FT properties still hold, others are modified. There fore it is not a surprise that Titchmarsh's theorem also hold for the QFT. To the best of our knowledge, Titchmarsh's theorem, the equivalence of a K-functional and the modulus of smoothness for the QFT have not derived yet. In this Paper is extended the Titchmarsh's theorem in the frame of quaternion analysis and it is proved the equivalence of a K-functional and the modulus of smoothness using the Steklovs function. Recall that the relation between smoothness conditions imposed on functions $f(x)$ and the behavior of its Fourier transforms f near infinity is well known in the literature. In fact, a classical result of Titchmarsh [29] says that

for $0 < \alpha \leq 1$, $1 < r \leq 2$ and

$$\left(\int_{\mathbb{R}} |f(x+h) - f(x)|^r dx \right)^{1/r} = O(h^{\alpha})$$

where $h \longrightarrow 0$, then the Fourier transform $\widehat{f}$ belongs to $L^{\beta}(\mathbb{R})$, for

$$\frac{r}{r+\alpha r-1} < \beta \leq \frac{r}{r-1}.$$

This theorem was extended to higher differences of functions in one and several variables in [33] and [34]. On the other hand, Younis in [32] studied the same phenomena for the wider Dini-Lipschitz class as well as for some other allied classes of functions. More precisely, he proved that if $f \in L^{r}(\mathbb{R})$, with $1 < r \leq 2$, such that

$$\left(\int_{\mathbb{R}} |f(x+h)-f(x)|^{r} dx\right)^{1/r} = O\left(\frac{h^{\alpha}}{log(\frac{1}{h})^{\gamma}}\right),$$

where $0 < \alpha \leq 1$, as $h \to 0$, then its Fourier transform $\widehat{f}$ belongs to $L^{\beta}(\mathbb{R})$, for

$$\frac{r}{r+\alpha r-1} < \beta \leq r' = \frac{r}{r-1}$$

and

$$\frac{1}{\beta} < \gamma.$$

In recent years, these two results have been generalized in several different versions and for several different types of transforms (for example, see [3, 12, 13]).
In addition, the usual translation operator τh given by $\tau hf(x) = f(x + h)$ plays a key role in the construction of modulus of continuity and smoothness which can be considered as a critical elements of direct and inverse theorems in approximation theory.
It is commonly known that studying the relation which exists between the smoothness properties of a function and the best approximations of this function in weight functional spaces is more convenient than usual with various generalized modulus of smoothness (see [26, 27]).
The K-functionals introduced by J. Peetre [25] take a part in a many problems of theory of approximation of functions. The study of the relation which exists between the modulus of smoothness and K-functionals is known as one of the major problems in the theory of approximation of functions . For many generalized modulus of smoothness these problems are studied, for example, in [4, 11, 14].

In order to describe our results, we first need to introduce some facts about harmonic analysis related to (two-sided) Quaternion Fourier transform (QFT). We cite here, as briefly as possible, some properties. For more details we refer to [1, 2, 21, 22, 15, 23, 30, 31, 5, 10, 20].

The quaternion algebra H was first invented by W. R. Hamilton in 1843 for extending complex numbers to a 4D algebra [28]. A quaternion $q \in H$ can be written in this form

$$q = q0 + q = q0 + iq1 + jq2 + kq3$$

where i, j, k satisfy Hamilton's multiplication rules

$$i2 = ij2 = k2 = ijk = -1,\ ij = -ji = k.$$
$$jk = -kj = I,\ ki = -ik = j$$

Using Hamilton's multiplication rules, the multiplication of two quaternion $p = \underline{p0} + p$ *and* $q = q0 + \underline{q}$ can be expressed as

$$pq = p0q0 + p0\underline{q} + q0\underline{p} + \underline{pq}.$$

We define so, the conjugation of $q \in \mathcal{H}$ by $\overline{q} = q_0 - iq_1 - jq_2 - kq_3$. Clearly, $q\overline{q} = q_0^2 + q_1^2 + q_2^2 + q_3^2$. So the modulus of a quaternion q is defined by

$$|q| = \sqrt{q\overline{q}} = \sqrt{q_0^2 + q_1^2 + q_2^2 + q_3^2}.$$

In this paper, we study the quaternion-valued signal $f : \mathbb{R}^2 \to \mathcal{H}$ that can be expressed as

$$f = f_0 + if_1 + jf_2 + kf_3$$

where $x = x_1e_1 + x_2e_2 \in \mathbb{R}^2$ and $f_0,\ f_1,\ f_2$ and f_3 are real-valued functions. For $1 \leq r < \infty$, the quaternion modulus $L^r(\mathbb{R}^2, \mathcal{H})$ are defined as

$$L^r = L^r(\mathbb{R}^2, \mathcal{H}) = \{f/f : \mathbb{R}^2 \to \mathcal{H},\ \|f\|^r_{L^r(\mathbb{R}^2,\mathcal{H})} = \int_{\mathbb{R}^2} |f(x)|^r dx < \infty\ \}.$$

Let $f \in L^r(\mathbb{R}^2, \mathcal{H})$. The quaternion Fourier transform QFT of f is defined by

$$\mathcal{F}_Q(f)(\omega) = \frac{1}{2\pi} \int_{\mathbb{R}^2} e^{-ix_1\omega_1} f(x) e^{-jx_2\omega_2} dx.$$

Let $f \in L^r(\mathbb{R}^2, \mathcal{H})$. The quaternion Fourier transform QFT of f is defined by

$$\mathcal{F}_Q(f)(\omega) = \frac{1}{2\pi} \int_{\mathbb{R}^2} e^{-ix_1\omega_1} f(x) e^{-jx_2\omega_2} dx.$$

The inner product of $f, g \in L^2(\mathbb{R}^2, \mathcal{H})$ is defined by

$$\langle f, g\rangle = \int_{\mathbb{R}^2} f(x)\overline{g(x)} dx.$$

Clearly, $\|f\|_2^2 = \langle f, f\rangle$.

Now, we define $|.|_Q$ for $\mathcal{F}_Q(f)$ as

$$|\mathcal{F}_Q(f)(\omega)|_Q = \left(|\mathcal{F}_Q(f_0)(\omega)|^2 + |\mathcal{F}_Q(f_1)(\omega)|^2 + |\mathcal{F}_Q(f_2)(\omega)|^2 + |\mathcal{F}_Q(f_3)(\omega)|^2\right)^{1/2}.$$

For $f \in L^1(\mathbb{R}^2, \mathcal{H})$, we have

$$\|\mathcal{F}_Q(f)\|_{Q,\infty} \leq \|f\|_1. \tag{1}$$

(**Hausdorff-Young inequality**) If $1 \leq r < 2$ and letting r' be such that $1/r + 1/r' = 1$ then for all $f \in L^r(\mathbb{R}^2, \mathcal{H})$ it holds that

$$\|\mathcal{F}_Q(f)\|_{Q,r'} \leq \|f\|_r. \tag{4}$$

Suppose that $\mathcal{F}_Q(f) \in L^1(\mathbb{R}^2, \mathcal{H})$ and $\dfrac{\partial^{n+m} f}{\partial x_1^n \partial x_2^m} \in L^1(\mathbb{R}^2, \mathcal{H})$. Then

$$\mathcal{F}_Q\left(\frac{\partial^{n+m} f}{\partial x_1^n \partial x_2^m}\right)(w) = (iw_1)^n \mathcal{F}_Q(f)(w)(jw_2)^m,\ \ \forall n \in \mathbb{N}. \tag{5}$$

(**Shift property**) For a quaternion function $f \in L^1(\mathbb{R}^2, \mathcal{H})$, we denote by $\tau_k f(x)$ the shifted (translated) function defined by $\tau_k f(x) = f(x - k)$, where $k = k_1e_1 + k_1e_1 \in \mathbb{R}^2$. Then we obtain

$$\mathcal{F}_Q\{\tau_k f\}(\omega) = e^{ik_1\omega_1} \mathcal{F}_Q\{f\}(\omega_1, \omega_2) e^{jk_2\omega_2}. \tag{6}$$

For a function f on $L^1(\mathbb{R}^2, \mathcal{H})$ and for any $h_1, h_2 \in \mathbb{R}$, we define the operator Δ_{h_1,h_2} by

$$\Delta_{h_1,h_2} f(x) = f(x_1 + h_1, x_2 + h_2) - f(x_1 + h_1, x_2) - f(x_1, x_2 + h_2) + f(x_1, x_2). \tag{7}$$

Definition 1 *Let $f(x) = f(x_l, x_2)$ belongs to $L^r(\mathbb{R}^2, \mathcal{H})$, $1 \leq r < 2$. We say that f is in the Lipschitz space $Lip(\alpha_1, \alpha_2, r)$ if*

$$\|\Delta_{h_1,h_2} f(x)\|_r = O(h_1^{\alpha_1} h_2^{\alpha_2}), \tag{8}$$

as h_1, h_2 tend to zero, $1 \leq r < \infty$, $0 < \alpha_1, \alpha_2 \leq 1$.

In $L^2(\mathbb{R}^2, \mathcal{H})$, consider the operator

$$\varphi_h f(x_1, x_2) = \frac{1}{4h^2} \int_{-h}^{h} \int_{-h}^{h} f(x_1 + \xi, x_2 + \eta) d\xi d\eta. \tag{9}$$

Let the function $f \in L^2(\mathbb{R}^2, \mathcal{H})$. The finite differences of the order m ($m \in 1, 2, 3, ...$) are defined as follows:

$$\Delta_h^m f(x_1, x_2) = (I - \varphi_h)^m f(x_1, x_2),$$

here I is the unit operator, and the mth-order generalized continuity modulus of the function f is defined by the formula

$$e_m(f, \delta)_2 = \sup_{0<h<\delta} \|\Delta_h^m f\|_2,$$

where $\delta > 0$.
Consider in $L^2(\mathbb{R}^2, \mathcal{H})$ the operator

$$Df(x) = \left(\frac{\partial^2}{\partial x_1^2} + \frac{\partial^2}{\partial x_2^2} \right) f(x), \tag{10}$$

and $D^0 f = f$, $D^r f = D(D^{r-1} f)$, $r = 1, 2, ...$
In view of formulas (5) and (10), we have

$$\mathcal{F}_Q\{Df\}(w) = -\left(w_1^2 + w_2^2\right) \mathcal{F}_Q\{f\}(w),$$

and hence

$$\mathcal{F}_Q\{D^r f\}(w) = (-1)^r \left(w_1^2 + w_2^2\right)^r \mathcal{F}_Q\{f\}(w). \tag{11}$$

This leads to the following definition of K-functionals: for $t > 0$

$$K_m(f, t)_2 = \inf \left\{ \|f - g\|_2 + t\|D^m g\|_2, \;\; g \in W_2^m \right\},$$

where W_2^m is the Sobolev space constructed by the operator D,

$$W_2^m = \left\{ f \in L^2(\mathbb{R}^2, \mathcal{H}), D^r f \in L^2(\mathbb{R}^2, \mathcal{H}), r = 1, ..., m \right\}.$$

2. ON THE TITCHMARSH THEOREM FOR THE QUATERNION FOURIER TRANSFORM

Lipschitz classes have been constantly employed in Fourier analysis, although they appear in the realm of trigonometric series , more than they occur in Fourier transforms. There are several new results in this section including theorems for, higher differences more precisely we will give some results associated with Dini-Lipschitz Functions in *Lr ®2, H), 1 ≤r < 2* for quaternion Fourier Transform. We here prove the following

Theorem 1 *Let f belongs to $L^r(\mathbb{R}^2, \mathcal{H})$, $1 \leq r < 2$, and let f also belongs to $Lip(\alpha_1, \alpha_2, r)$. Then $|\mathcal{F}_Q(f)(\omega)|_Q$ belongs to L^β, where*

$$\frac{r}{r + \alpha_s r - 1} < \beta \leq \frac{r}{r - 1}, \;\; s = 1, 2.$$

Proof. By (7), we can show that the transform of $\Delta_{h_1,h_2} f(x)$ is given by

$$\mathcal{F}_Q(\Delta_{h_1,h_2} f(x)) = \left(e^{i\omega_1 h_1} - 1\right) \mathcal{F}_Q\{f\}(\omega) \left(e^{j\omega_2 h_2} - 1\right). \tag{12}$$

indeed

$$\begin{aligned} \mathcal{F}_Q(f(x_1 + h_1, x_2 + h_2)) &= e^{i\omega_1 h_1} \mathcal{F}_Q\{f\}(\omega) e^{j\omega_2 h_2} \\ \mathcal{F}_Q(f(x_1 + h_1, x_2)) &= e^{i\omega_1 h_1} \mathcal{F}_Q\{f\}(\omega) \\ \mathcal{F}_Q(f(x_1, x_2 + h_2)) &= \mathcal{F}_Q\{f\}(\omega) e^{j\omega_2 h_2} \end{aligned}$$

thus

$$\begin{aligned} \mathcal{F}_Q(\Delta_{h_1,h_2} f(x)) &= e^{i\omega_1 h_1} \mathcal{F}_Q\{f\}(\omega) e^{j\omega_2 h_2} - e^{i\omega_1 h_1} \mathcal{F}_Q\{f\}(\omega) - \mathcal{F}_Q\{f\}(\omega) e^{j\omega_2 h_2} + \mathcal{F}_Q\{f\} \\ &= e^{i\omega_1 h_1} \mathcal{F}_Q\{f\}(\omega)(e^{j\omega_2 h_2} - 1) - \mathcal{F}_Q\{f\}(\omega)(e^{j\omega_2 h_2} - 1) \end{aligned}$$

which gives the desired result. As well, we can easily obtain that

$$e^{i\omega_1 h_1} - 1 = 2ie^{i\frac{\omega_1 h_1}{2}} \sin\frac{\omega_1 h_1}{2}$$

and

$$e^{j\omega_2 h_2} - 1 = 2je^{j\frac{\omega_2 h_2}{2}} \sin\frac{\omega_2 h_2}{2}.$$

Hence

$$|\mathcal{F}_Q(\Delta_{h_1,h_2} f(x))|_Q = 4|\sin(\frac{\omega_1 h_1}{2})||\mathcal{F}_Q\{f\}(\omega)|_Q|\sin(\frac{\omega_2 h_2}{2})|.$$

by (4) and (8) we get that

$$\int_{\mathbb{R}^2} |\sin(\frac{\omega_1 h_1}{2})|^{r'} |\sin(\frac{\omega_2 h_2}{2})|^{r'} |\mathcal{F}_Q\{f\}(\omega)|_Q^{r'} d\omega_1 d\omega_2 = O(h_1^{\alpha_1 r'} h_2^{\alpha_2 r'}). \tag{13}$$

We obtain

$$\int_0^{\frac{2}{h_1}} \int_0^{\frac{2}{h_2}} |\frac{\omega_1 h_1}{2}|^{r'} |\frac{\omega_2 h_2}{2}|^{r'} |\mathcal{F}_Q\{f\}(\omega)|_Q^{r'} d\omega_1 d\omega_2 = O(h_1^{\alpha_1 r'} h_2^{\alpha_2 r'}),$$

it follows that

$$\int_0^{\frac{2}{h_1}} \int_0^{\frac{2}{h_2}} |\omega_1\omega_2|^{r'} |\mathcal{F}_Q\{f\}(\omega)|_Q^{r'} d\omega_1 d\omega_2 = O(h_1^{(\alpha_1-1)r'} h_2^{(\alpha_2-1)r'}).$$

Thus

$$\int_0^X \int_0^Y |\omega_1\omega_2|^{r'} |\mathcal{F}_Q\{f\}(\omega)|_Q^{r'} d\omega_1 d\omega_2 = O(X^{(1-\alpha_1)r'} Y^{(1-\alpha_2)r'}).$$

Now, we need to introduce the function ψ defined by

$$\psi(X, Y) = \int_1^X \int_1^Y |\omega_1\omega_2|^{\beta} |\mathcal{F}_Q\{f\}(\omega)|_Q^{\beta} d\omega_1 d\omega_2.$$

By the Hlder inequality, for $\beta \leq r'$ we get that

$$\psi(X, Y) = O(X^{1-\alpha_1\beta+\frac{\beta}{r}} Y^{1-\alpha_2\beta+\frac{\beta}{r}}),$$

so that

$$\int_1^X \int_1^Y |\mathcal{F}_Q\{f\}(\omega)|_Q^{\beta} d\omega_1 d\omega_2 = O(X^{1-\beta-\alpha_1\beta+\frac{\beta}{r}} Y^{1-\beta-\alpha_2\beta+\frac{\beta}{r}}).$$

This quantity is bounded as $X, Y \to \infty$ if $1-\beta-\alpha_1\beta+\frac{\beta}{r}<0$ and $1-\beta-\alpha_2\beta+\frac{\beta}{r}<0$, i.e.

$$\frac{r}{r+\alpha_1 r-1}<\beta \ \text{ and } \ \frac{r}{r+\alpha_2 r-1}<\beta,$$

and the proof is complete. ■

Theorem 2 *Let f belongs to $L^r(\mathbb{R}^2,\mathcal{H})$, $1\le r<2$, and let*

$$\|\Delta_{h_1,h_2}f(x)\|_r = O\left(\frac{h_1^{\alpha_1}}{\log(\frac{1}{h_1})^{\gamma_1}}.\frac{h_2^{\alpha_2}}{\log(\frac{1}{h_2})^{\gamma_1}}\right),\ \ 0<\alpha_1,\alpha_2<1,\ \ as\ \ h_1,h_2\to\infty. \tag{14}$$

Then $|\mathcal{F}_Q(f)(\omega)|_Q \in L^\beta$ for

$$\frac{r}{r+\alpha_s r-1}<\beta\le\frac{r}{r-1},\ \ \beta>\frac{1}{\gamma_s},\ \ s=1,2. \tag{15}$$

Proof. By analogy with the proof of the Theorem (1), we can establish the following result

$$\int_{\mathbb{R}^2}|\sin(\frac{\omega_1 h_1}{2})|^{r'}|\sin(\frac{\omega_2 h_2}{2})|^{r'}|\mathcal{F}_Q\{f\}(\omega)|_Q^{r'}d\omega_1 d\omega_2 = \left(\frac{h_1^{\alpha_1 r'}}{\log(\frac{1}{h_1})^{\gamma_1 r'}}.\frac{h_2^{\alpha_2 r'}}{\log(\frac{1}{h_2})^{\gamma_1 r'}}\right). \tag{16}$$

If $0<\omega_s<\frac{2}{h_s}$, $s=1,2$, then $|\frac{\omega_s h_s}{2}|<A|\sin(\frac{\omega_s h_s}{2})|$, A being constant and therefore

$$\int_0^{\frac{2}{h_1}}\int_0^{\frac{2}{h_2}}|\omega_1\omega_2|^{r'}|\mathcal{F}_Q\{f\}(\omega)|_Q^{r'}d\omega_1 d\omega_2 = \left(\frac{h_1^{(\alpha_1-1)r'}}{\log(\frac{1}{h_1})^{\gamma_1 r'}}.\frac{h_2^{(\alpha_2-1)r'}}{\log(\frac{1}{h_2})^{\gamma_1 r'}}\right).$$

Thus

$$\int_0^X\int_0^Y|\omega_1\omega_2|^{r'}|\mathcal{F}_Q\{f\}(\omega)|_Q^{r'}d\omega_1 d\omega_2 = \left(\frac{X^{(1-\alpha_1)r'}}{\log(X)^{\gamma_1 r'}}.\frac{Y^{(1-\alpha_2)r'}}{\log(Y)^{\gamma_1 r'}}\right).$$

Let

$$\phi(X,Y)=\int_1^X\int_1^Y|\omega_1\omega_2|^{\beta}|\mathcal{F}_Q\{f\}(\omega)|_Q^{\beta}d\omega_1 d\omega_2.$$

For $\beta\le r'$ and by the Hölder inequality, we obtain

$$\phi(X,Y)=O\left(\frac{X^{1-\alpha_1\beta+\frac{\beta}{r}}}{\log(X)^{\gamma_1\beta}}\frac{Y^{1-\alpha_2\beta+\frac{\beta}{r}}}{\log(Y)^{\gamma_2\beta}}\right),$$

it follows that

$$\int_1^X\int_1^Y|\mathcal{F}_Q\{f\}(\omega)|_Q^{\beta}d\omega_1 d\omega_2 = O\left(\frac{X^{1-\beta-\alpha_1\beta+\frac{\beta}{r}}}{\log(X)^{\gamma_1\beta}}\frac{Y^{1-\beta-\alpha_2\beta+\frac{\beta}{r}}}{\log(Y)^{\gamma_2\beta}}\right),$$

and for the right hand of this estimate to be bounded as $X, Y\to\infty$ one must have

$$1-\beta-\alpha_1\beta+\frac{\beta}{r}<0,\ \ -\gamma_1\beta<-1$$

and

$$1-\beta-\alpha_2\beta+\frac{\beta}{r}<0,\ \ -\gamma_2\beta<-1,$$

then

$$\frac{r}{r+\alpha_s r-1}<\beta,\ \ \beta>\frac{1}{\gamma_s},\ \ s=1,2.$$

This completes the proof. ■

In the next we study if the proceeding theorems are still valid if we replace the first difference $\Delta_{h_1,h_2}f$ with a difference of higher order. We put

$$\Delta^{n,m}_{h_1,h_2}f(x)=\sum_{k_2=0}^{m}\sum_{k_1=0}^{n}(-1)^{n-k_1}(-1)^{m-k_2}\binom{n}{k_1}\binom{m}{k_2}f(x_1+k_1h_1,x_2+k_2h_2). \tag{17}$$

Observe that $\Delta^{1,1}_{h_1,h_2}f(x)=\Delta_{h_1,h_2}f(x)$. We now generalize Theorem 1 as follows.

Theorem 3 *If $f\in L^r(\mathbb{R}^2,\mathcal{H})$, $1\leq r<2$, and if*

$$\|\Delta^{n,m}_{h_1,h_2}f(x)\|_r=O(h_1^{\alpha_1}h_2^{\alpha_2}),\ \ 0<\alpha_1<n,0<\alpha_2<m\ \ as\ \ h_1,h_2\to\infty, \tag{18}$$

then $|\mathcal{F}_Q(f)(\omega)|_Q\in L^\beta$, where

$$\frac{r}{r+\alpha_s r-1}<\beta\leq\frac{r}{r-1},\ \ s=1,2.$$

Proof. For two fixed h_1 and h_2, the transform of $\Delta^{n,m}_{h_1,h_2}f(x)$ is given

$$\left(\sum_{k_1=0}^{n}(-1)^{n-k_1}\binom{n}{k_1}e^{ik_1\omega_1h_1}\right)\mathcal{F}_Q\{f\}(\omega)\left(\sum_{k_2=0}^{m}(-1)^{m-k_2}\binom{m}{k_2}e^{jk_2\omega_2h_2}\right). \tag{19}$$

We can easily get that

$$\sum_{k_1=0}^{n}(-1)^{n-k_1}\binom{n}{k_1}e^{ik_1\omega_1h_1}=\left(e^{i\omega_1h_1}-1\right)^n=(2i)^ne^{in\frac{\omega_1h_1}{2}}\left(\sin\frac{\omega_1h_1}{2}\right)^n$$

and

$$\sum_{k_2=0}^{m}(-1)^{m-k_2}\binom{m}{k_2}e^{jk_2\omega_2h_2}=\left(e^{j\omega_2h_2}-1\right)^m=(2j)^me^{jm\frac{\omega_2h_2}{2}}\left(\sin\frac{\omega_2h_2}{2}\right)^m.$$

which yields

$$|\mathcal{F}_Q(\Delta^{n,m}_{h_1,h_2}f(x))|_Q=2^{n+m}|\sin(\frac{\omega_1h_1}{2})|^n|\mathcal{F}_Q\{f\}(\omega)|_Q|\sin(\frac{\omega_2h_2}{2})|^m.$$

By (4) we obtain

$$\int_{\mathbb{R}^2}|\sin(\frac{\omega_1h_1}{2})|^{nr'}|\sin(\frac{\omega_2h_2}{2})|^{mr'}|\mathcal{F}_Q\{f\}(\omega)|_Q^{r'}d\omega_1d\omega_2=O(h_1^{\alpha_1r'}h_2^{\alpha_2r'}). \tag{20}$$

So that

$$\int_0^{\frac{2}{h_1}}\int_0^{\frac{2}{h_2}}|\omega_1|^{nr'}\omega_2|^{mr'}|\mathcal{F}_Q\{f\}(\omega)|_Q^{r'}d\omega_1d\omega_2=O(h_1^{(\alpha_1-n)r'}h_2^{(\alpha_2-m)r'}),$$

which gives the desired result. ■

We shall also generalize Theorem 2 to the following theorem

Theorem 4 *If f belongs to $L^r(\mathbb{R}^2,\mathcal{H})$, $1\leq r<2$, and if*

$$\|\Delta^{n,m}_{h_1,h_2}f(x)\|_p=O\left(\frac{h_1^{\alpha_1}}{\log(\frac{1}{h_1})^{\gamma_1}}.\frac{h_2^{\alpha_2}}{\log(\frac{1}{h_2})^{\gamma_1}}\right),\ \ 0<\alpha_1<n,0<\alpha_2<m\ \ as\ \ h_1,h_2\to\infty, \tag{21}$$

then $|\mathcal{F}_Q(f)(\omega)|_Q\in L^\beta$, where (15) holds.

Proof. The proof for this theorem is very similar to the proof of Theorem (3)and then

$$\int_0^{\frac{2}{h_1}} \int_0^{\frac{2}{h_2}} |\omega_1|^{mr'} |\omega_2|^{mr'} |\mathcal{F}_Q\{f\}(\omega)|_Q^{p'} d\omega_1 d\omega_2 = \left(\frac{h_1^{(\alpha_1 - n)r'}}{\log(\frac{1}{h_1})^{\gamma_1 r'}} \cdot \frac{h_2^{(\alpha_2 - m)r'}}{\log(\frac{1}{h_2})^{\gamma_1 r'}} \right).$$

The rest of the proof is now analogous to the proof of Theorem 2 and (15) holds. ■

3. EQUIVALENCE OF A K-FUNCTIONAL AND THE MODULUS OF SMOOTHNESS FOR QUATERNION FOURIER TRANSFORM

Modulus of smoothness represent important tools in obtaining quantitative estimates of the error of approximation for positive processes. There are many such special functions associated with wide classes of function spaces. On another hand , in many problems of the theory of approximation of functions the K-functionals play an important role. The study of the connection between the modulus of smoothness and K-functionals is one of the main problems in the theory of approximation of functions. For various generalized modulus of smoothness these problems are studied, for example, in [9, 19].
In order to prove the main result, we shall need some preliminary results.

Lemma 1 *If f belongs to $L^2(\mathbb{R}^2, \mathcal{H})$, then*

$$\|\Delta_h^m f\|_2 \leq 2^m \|f\|_2. \tag{22}$$

Proof. Using the inequality (9), we have $\|\varphi_h f\|_2 \leq \|f\|_2$. Then $\|\Delta_h^1 f\|_2 \leq 2\|f\|_2$. Thus the result follows easily by using the recurrence for m. ■

Lemma 2 *If quaternion function $f \in L^2(\mathbb{R}^2, \mathcal{H})$, then*

$$\mathcal{F}_Q\{\varphi_h f\}(w) = \frac{\sin(w_1 h)}{w_1 h} \frac{\sin(w_2 h)}{w_2 h} \mathcal{F}_Q\{f\}(w). \tag{23}$$

Proof. Let $f \in L^2(\mathbb{R}^2, \mathcal{H})$, we have

$$\mathcal{F}_Q\{\varphi_h f\}(w) = \frac{1}{4h^2} \int_{-h}^{h} \int_{-h}^{h} e^{i\omega_1 \xi} \mathcal{F}_Q\{f\}(\omega) e^{j\omega_2 \eta} d\xi d\eta$$

$$= \left(\frac{1}{2h} \int_{-h}^{h} e^{i\omega_1 \xi} d\xi \right) \mathcal{F}_Q\{f\}(\omega) \left(\frac{1}{2h} \int_{-h}^{h} e^{j\omega_2 \eta} d\eta \right).$$

Since

$$\frac{1}{2h} \int_{-h}^{h} e^{i\omega_1 \xi} d\xi = \frac{\sin(w_1 h)}{w_1 h}$$

and

$$\frac{1}{2h} \int_{-h}^{h} e^{j\omega_2 \eta} d\eta = \frac{\sin(w_2 h)}{w_2 h}.$$

So that the transform of $\varphi_h f(x)$ is given as

$$\frac{\sin(w_1 h)}{w_1 h} \frac{\sin(w_2 h)}{w_2 h} \mathcal{F}_Q\{f\}(w).$$

Which gives the desired result. ■

corollaire 1 *For any function f belongs to $L^2(\mathbb{R}^2, \mathcal{H})$, we have*

$$\mathcal{F}_Q\{\Delta_h^m f\}(w) = \left(1 - \frac{\sin(w_1 h)}{w_1 h}\frac{\sin(w_2 h)}{w_2 h}\right)^m \mathcal{F}_Q\{f\}(w). \tag{24}$$

Lemma 3 *Let f belongs to $L^2(\mathbb{R}^2, \mathcal{H})$ and $t > 0$. Then*

$$e_m(f,t)_2 \leq \frac{1}{6^m} t^{2m} \parallel D^m f \parallel_2 . \tag{25}$$

Proof. Let $h \in (0, t]$. By (11), (24) and the Parseval equality, we get

$$\parallel \Delta_h^m f \parallel_2 = \parallel \left(1 - \frac{\sin(w_1 h)}{w_1 h}\frac{\sin(w_2 h)}{w_2 h}\right)^m \mathcal{F}_Q\{f\}(w) \parallel_2 \tag{26}$$

and

$$\parallel D^m f \parallel_2 = \parallel \left(w_1^2 + w_2^2\right)^m \mathcal{F}_Q\{f\} \parallel_2 . \tag{27}$$

Hence, by (26) and (27) it follows that

$$\parallel \Delta_h^m f \parallel_2 = h^{2m} \parallel \left(\frac{1 - \frac{\sin(w_1 h)}{w_1 h}\frac{\sin(w_2 h)}{w_2 h}}{w_1^2 + w_2^2}\right)^m \left(w_1^2 + w_2^2\right)^m \mathcal{F}_Q\{f\}(w) \parallel_2 .$$

Since

$$0 \leq 1 - \frac{\sin(y)}{y} \leq \frac{y^2}{6}, \quad |\sin(y)| \leq |y|, \quad y \in \mathbb{R},$$

and

$$1 - \frac{\sin(w_1 h)}{w_1 h}\frac{\sin(w_2 h)}{w_2 h} = \left(1 - \frac{\sin(w_1 h)}{w_1 h}\right)\frac{\sin(w_2 h)}{w_2 h} + \left(1 - \frac{\sin(w_2 h)}{w_2 h}\right),$$

we obtain

$$0 \leq 1 - \frac{\sin(w_1 h)}{w_1 h}\frac{\sin(w_2 h)}{w_2 h} \leq \frac{1}{6}\left((w_1 h)^2 + (w_2 h)^2\right).$$

Thus

$$\parallel \Delta_h^m f \parallel_2 \leq \frac{1}{6^m} h^{2m} \parallel \left(w_1^2 + w_2^2\right)^m \mathcal{F}_Q\{f\}(w) \parallel_2 .$$

This combined with (27), we have

$$\parallel \Delta_h^m f \parallel_2 \leq \frac{1}{6^m} h^{2m} \parallel D^m f \parallel_2 \leq \frac{1}{6^m} t^{2m} \parallel D^m f \parallel_2,$$

which gives the desired result. ■

Now, given $\nu > 0$, We introduce the following operator for $f \in L^2(\mathbb{R}^2, \mathcal{H})$ by

$$Q_\nu(f)(x) = \mathcal{F}_Q^{-1}\{\mathcal{F}_Q(f)(\omega)\mathbb{I}_\nu(\omega)\}(x),$$

where $\mathbb{I}_\nu(\lambda)$ is the characteristic function of the segment $[-\nu, \nu]$.

It is easy to show that the function $Q_\nu(f)$ is infinitely differentiable and belongs to all classes W_2^m, $m \in \{1, 2, 3, ...\}$.

Lemma 4 *If f belongs to $L^2(\mathbb{R}^2, \mathcal{H})$ and $\nu > 0$. Then there exists a positive constant c_2 such that*

$$\|f - Q_\nu(f)\|_2 \leq c_2 \|\Delta_{1/\nu}^m f\|_2. \tag{28}$$

Let

$$c_3 = \sup_{|\xi|\leq 1} \left\{ \frac{\left(\xi_1^2+\xi_2^2\right)^m}{\left(1-\frac{\sin(\xi_1)}{\xi_1}\frac{\sin(\xi_2)}{\xi_2}\right)^m} \right\},$$

which is exactly (30), and it is clear that the formula (30) yields the inequality (31). ■

Theorem 5 *Let f belongs to $L^2(\mathbb{R}^2,\mathcal{H})$ and $\delta>0$. One can find positive constant c_4 such that*

$$\frac{1}{2^m}e_m(f,\delta)_2 \leq K_m(f,\delta^{2m})_2 \leq c_4 e_m(f,\delta)_2. \tag{32}$$

Proof. Let $h\in(0,\delta]$ and $g\in W_2^m$. Using Lemma 1 and 3, we deduce

$$\begin{aligned}\|\Delta_h^m f\|_2 &\leq \|\Delta_h^m(f-g)\|_2+\|\Delta_h^m g\|_2\\ &\leq 2^m\|f-g\|_2+\frac{1}{6^m}h^{2m}\parallel D^m g\parallel_2\\ &\leq 2^m(\|f-g\|_2+\delta^{2m}\parallel D^m g\parallel_2).\end{aligned}$$

Calculating the supremum with respect to $h\in(0,\delta]$ and the infimum with respect to all possible functions $g\in W_2^m$, we obtain

$$e_m(f,\delta)_2 \leq 2^m K_m(f,\delta^{2m})_2.$$

Since $Q_\nu(f)\in W_m^2$, by the definition of of a K-functional, it follows that

$$K_m(f,\delta^{2m})_2 \leq \|f-Q_\nu(f)\|_2+\delta^{2m}\parallel D^m Q_\nu(f)\parallel_2 .$$

Therefore, using (29) and (31), we have

$$K_m(f,\delta^{2m})_2 \leq c_2 e_m(f,1/\nu)_2 + c_3(\delta\nu)^{2m}e_m(f,1/\nu)_2.$$

Putting $\nu=\dfrac{1}{\delta}$ in this inequality, we deduce

$$K_m(f,\delta^{2m})_2 \leq c_4 e_m(f,\delta)_2,$$

where $c_4=c_2+c_3$. This concludes the proof of Theorem 5. ■

REFERENCES

[1] Achak, A., Abouelaz, A., Daher, R. et al, Uncertainty Principles for The Quaternion Linear Canonical Transform. Adv. Appl. Clifford Algebras (2019) 29: 99.

[2] A. Abouelaz,A. Achak, R. Daher and N. Safouane, Donoho-Stark's uncertainty principle for the quaternionFourier transform, Bol. Soc. Mat. Mex. (2019). https://doi.org/10.1007/s40590-019-00251-5

[3] A. Abouelaz, R. Daher, M. El Hamma. Fourier transform of Dini-Lipschitz functions in the space, Roman.J. Math. Comput. Sci. 3, 41-47 (2013).

[4] E.S. Belkina and S.S. Platonov, Equivalence of K-functionnals andmodulus of smoothness constructed by generalized dunkl translations, Izv. Vyssh. Uchebn. Zaved. Mat. 8 (2008) 3-15.

[5] M. Bahri a,1, H. Eckhard , A. Hayashi a, R. Ashino, An uncertainty principle for quaternion Fouriertransform, Computers and Mathematics with Applications 56 (2008) 2398-2410.

[6] M. Bahri and F. M. Saleh Arif, Relation between Quaternion Fourier Transform and Quaternion Wigner Ville Distribution Associated with Linear Canonical Transform, Journal of AppliedMathematics, vol. 2017,Article ID 3247364.

[7] R. Bracewell, The Fourier Transform and its Applications, third ed., McGraw-Hill Book Company, New York, 2000.
[8] T. Blow, Hypercomplex spectral signal representations for the processing and analysis of images, Ph.D.Thesis, Institut fr Informatik und Praktische Mathematik, University of Kiel, Germany, 1999.
[9] P. L. Butzer and R.J. Nessel, Fourier Analysis and Approximation, Vol. l. Birkauser Verlag, Basel, 1971.
[10] L.-P. Chen K. I. Kou M.-S. Liu, Pitt's inequality and the uncertainty principle associated with the quaternion Fourier transform, J. Math. Anal. Appl. (2015).[11] Feng Dai, Some Equivalence Theorems with K-Functionals, J. Appr. Theory 121, 143-157 (2003).
[12] R. Daher and M. Hamma, Bessel Transform of (k, γ)−Bessel Lipschitz Functions, Hindawi Publishing Corporation Journal of Mathematics Vol. 2013, Article ID 418546, 3 pages.
[13] R. Daher and M. Hamma, Dunkl transform of Dini-Lipschitz functions, Electronic Journal of Mathematical Analysis and Applications Vol. 1. No. 2, pp. 1-6 (2013).
[14] Z. Ditzian and V. Totik, Moduli of Smoothness, Moduli of Smoothness (Springer-Verlag, New York etc., 1987).
[15] Y. El Haoui and S. Fahlaoui, The Uncertainty principle for the two-sided quaternion Fouriertransform,Mediterr. J. Math. (2017) doi:10.1007/s00009-017-1024-5
[16] M. Felsberg, Low-Level image processing with the structure multivector, Ph.D. Thesis, Institut fr Informatik und Praktische Mathematik, University of Kiel, Germany, 2002.
[17] X. Guanlei, W. Xiaotong, and X. Xiaogang, Fractional quaternion fourier transform, convolution and correlation, Signal Processing, 88(10), 25112517 (2008).
[18] L. Guo, M. Zhu, and X. Ge, Reduced biquaternion canonical transform, convolution and correlation, Signal Processing, 91(8), 21472153(2011).
[19] T. L. Hayden and J.H. Wells, on the extension of Lipschitz-Holder maps of order β, J. Math. Analysis and Applications, 33 (1971) 627-640.
[20] E. Hitzer, Quaternion Fourier transform on quaternion fields and generalizations, Advances in Applied Clifford Algebras 17 (3) (2007) 497-517.
[21] B. Hu,Y.Zhou, L. D. Lie, and J.Y.Zhang, Polar linear canonical transform in quaternion domain, Journal of Information Hiding and Multimedia Signal Processing, vol. 6, no. 6, pp. 1185-1193, 2015.
[22] K. I. Kou, J.-Y.Ou, and J.Morais, On uncertainty principle for quaternionic linear canonical transform, Abstract and Applied Analysis, vol. 2013, Article ID 725952, 14 pages, 2013.
[23] K. I. Kou and J. Morais, Asymptotic behaviour of the quaternion linear canonical transform and the Bochner-Minlos theorem, Applied Mathematics and Computation, vol. 247, no. 15, pp. 675-688, 2014.
[24] K. I. Kou, J. Y. Ou, and J. Morais, On uncertainty principle for quaternionic linear canonical transform, in Abstract and Applied Analysis, Hindawi Publishing Corporation, Article ID 725952, 2013,14, (2013).
[25] J. Peetre, A Theory of Interpolation of Normed Spaces,Notes de Universidade de Brasilia, 1963.
[26] Mk. Potapov, Application of the Operator of Generalized Translation in Approximation Theory,Vestnik Moskovskogo Universiteta, Seriya Matematika, Mekhanika, 3 (1998), 38-48.
[27] S.S. Platonov, Generalized Bessel Translations and Certain Problems of the Theory of Approximation of Functions in the Metrics of L2,α.I,Trudy Petrozavodskogo Gosudarstvennogo Universiteta, Seriya Matematika, 7 (2000), 70-82.
[28] A. Sudbery, Quaternionic analysis, Math. Proc. Cambridge Phil. Soc. 85: 199- 225 (1979).
[29] E.C. Titchmarsh, Introduction to the theory of Fourier Integrals, pp. 115–118. Clarendon Press, Oxford(1937).
[30] Q. Xiang and K-. Y. Qin, On the relationship between the linear canonical transform and the

Fourier transform, 2011 4th International Congress on Image and Signal Processing (CISP), 2214-2217.
[31] Y. Yang and K. I. Kou, Uncertainty principles for hypercomplex signals in the linear canonical transform domains, Signal Processing, vol. 95, pp. 67-75, 2014.
[32] M.S. Younis, Fourier transforms of Dini-Lipschitz Functions, Int. J. Math. Math. Sci. 9(2), 301–312 (1986).
[33] M.S. Younis, Fourier Transforms on L p Spaces, Int. J. Math. Math. Sci. 9(2), 301–312 (1986).
[34] M.S. Younis, Fourier Transforms of Lipschitz Functions on Compact Groups, Ph. D. Thesis. McMaster University (Hamilton, Ont., Canada, 1974).

Lithium-ion battery modeling using equivalent circuit model

ER-RAKIBI Marwane1
1Master, Materials and Radiation, Energy and Environment
Faculty of Sciences, Chouaïb Doukkali University, El Jadida, Morocco

A B S T R A C T

With modern technologies, most devices such as electric vehicles are powered by lithium batteries. This kind of battery is advantageous to other types of batteries, such as higher energy density, reliability, etc. to work effectively, it is necessary to handle them using a battery management system BMS, which guarantees their safety and optimizes their performances in normal conditions. One of the things that a BMS must do is to estimate the state of charge SOC of the battery because it is the most critical indicator of battery state. This task is very challenging because the lithium-ion battery is a highly time-invariant, nonlinear, and complex electrochemical system. In this paper, we present a cell model that can be used in the state of the charge estimation process. This model is based on an electrical approach where we build an electrical circuit that has the same behavior as the real cell, this approach is called the Equivalent circuit model ECM. using a set of laboratory data, we will determine the model parameters using multiple techniques. Those parameters will be used in process of estimating the state of charge and other internal parameters.

Keywords: Lithium-ion Battery , Battery Modelling, Equivalent circuit model, BMS

1. INTRODUCTION

The battery system is the most important energy storage source in electric vehicles (EVs) [1]. These days, the development trend in the field of electric vehicles is the use of high-capacity lithium-ion batteries as a battery energy storage system [2]. This kind of battery presents multiple benefits such as high-power density, lightweight, long life, and thermal stability.

To prolong the lifetime and increase the safety of these batteries, it is essential to monitor their state of charge in real-time. This task is performed by battery management systems that control, optimize and protect the battery. One of the main tasks of a battery management system is to estimate the number of fundamental quantities, such as the state of charge SOC of the cell, the state of health SOH of the cell battery, available power, and available energy. The best methods to produce these estimates require models that describe the dynamic behavior of the cell with precision.

Since the SOC cannot be measured directly, many approaches have been proposed to estimate the SOC of the battery [3–6]. One of those approaches is called model-based estimation of the state of charge, this approach is widely used in the application for its high accuracy and self-corrective ability [7–9]. One of the cell models that can be used to perform such an operation, is the equivalent circuit model ECM.

ECMs represent the operation of a lithium-ion cell by providing an electrical circuit, which behaves the same as cells. Data collected from cells via laboratory tests are used to optimize the parameter values of the proposed circuit elements so that the current and voltage behaviors of the model match exactly those of the real cell. [10]

In the rest of this paper, we adopt the equivalent circuit model approach, where we build the model circuit element by element, starting with an explanation of the observed dominant behavior. Any difference between the model predictions and the observed behavior of the cells is therefore considered to be a modeling error.

2. LITHIUM-ION CELL MODELLING

Open circuit voltage OCV

We begin the cell modeling by explaining the most observed behavior of the battery cell. This model, figure (1), presents the cell as an ideal voltage source v(t). Indeed, the cell delivers a voltage to its terminals. This voltage is measured by a voltmeter, where we notice that it is constant, and is not a function of the current flowing in the load connected to the cell. This model is simple and it's very different from the reality where OCV depends on the cell state of charge.

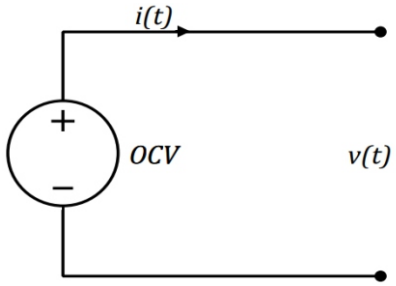

Figure 1. Cell ideal model diagram where open circuit voltage has a constant value.

State of charge effect on OCV

The first improvement that we make to the simple cell model is due to the difference in voltages in a cell with different states of charge. Indeed, we notice that the cell voltage at equilibrium or the OCV of a fully charged cell is greater than the OCV of a fully discharged cell.

The improved cell model, Figure (2), includes OCV dependence on the state of charge of the cell. The ideal voltage source is replaced by a controlled voltage source, which has a value equal to OCV (z (t)), where z(t) is the state of charge of the cell. If we take into account the dependence of the OCV on temperature, we use the notation OCV (z (t), T (t)), where T (t) is the internal temperature of the cell as a function of time.

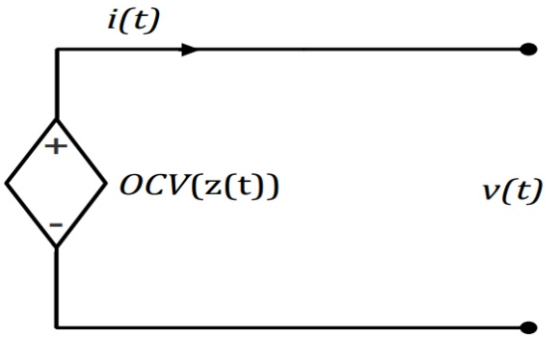

Figure 2. Cell model diagram including OCV dependence on the state of charge.

We can model the state of charge changes using the following differential equation:

$$\frac{dz(t)}{dt} = -\frac{\eta(t)i(t)}{Q}, \#(1)$$

where z (t) represents the state of charge, η (t) the Coulomb efficiency or the charging efficiency, Q the total capacity. When the cell is being discharged, the current i(t) is positive and η(t) takes the value of 1, which leads to the decrease of z (t). On the other hand, z (t) increases at the charge of the cell where the

current is negative and the Coulomb efficiency is $\eta(t) \leq 1$.

By integrating the equation (1) between time t0 and t and if we assume that the current is constant over the sampling interval, then we have:

$$z(t) = z(t0) - \frac{1}{Q}\int_{t0}^{t} \eta(t)i(t)dt \#(2)$$

This equation must be written in discrete-time so we can use it in numerical calculus. To do so, let $t0 = k\Delta t$ et $t = (k+1)\Delta t$. so:

$$z\big((k+1)\Delta t\big) = z(k\Delta t) - \frac{\Delta t}{Q}\eta(k\Delta t)i(k\Delta t)\#(3)$$

Finally:

$$\boldsymbol{z[k+1] = [z] - \frac{\Delta t}{Q}\eta[k]i[k]\#(4)}$$

Equivalent series resistance

The first observation we notice is that when the cell powers an external load, the voltage across its terminals drops below the open-circuit voltage OCV (z(t)), and when the cell is being charged, the voltage at these terminals rises above the open circuit voltage OCV (z (t)). This phenomenon can be explained by placing a resistor in series with the voltage source. The new model is shown in the diagram in figure (3). The resistance added to the diagram represents what is called the equivalent series resistance (ESR) of the cell. The reason we choose this circuit over others is that the behavior observed in this case is similar to the response of the chosen circuit, where the voltage v(t) drops than OCV(z(t)) due to the presence of the resistor R0.

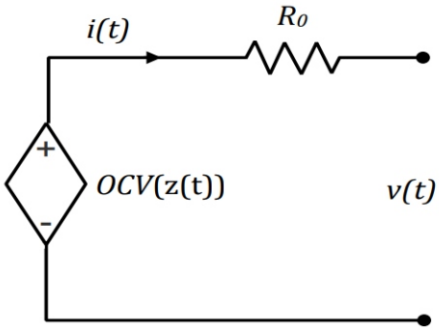

Figure 3. Cell model diagram including the equivalent series resistance.

In the new model, the state of charge equation remains unchanged. However, we add a second equation to the model which describes the voltage across the circuit.

In continuous time:

$$v(t) = OCV\big(z(t)\big) - i(t)R_0\#(5)$$

In discrete time

$$v[k] = OCV\,(z[k]) - i[k]R_0\#(6)$$

Polarization effect

Polarization in the cell refers to any deviation between the voltage across the cell from the open-circuit voltage OCV(z(t)), due to current flow through the cell. In the equivalent circuit model that we have developed so far, we have modeled the instantaneous bias via the term i (t) × R0. Real cells have more complex behavior, where the voltage bias increases slowly over time when current is demanded from the cell, and then slowly decreases over time when the cell is allowed to rest.

This phenomenon is caused by the slow diffusion processes of lithium in a lithium-ion cell, this slowly changing voltage is called, the diffusion voltage. Its effect can be approximated in a circuit by using one or more resistor-capacitor sub-circuits in parallel. Figure (4).

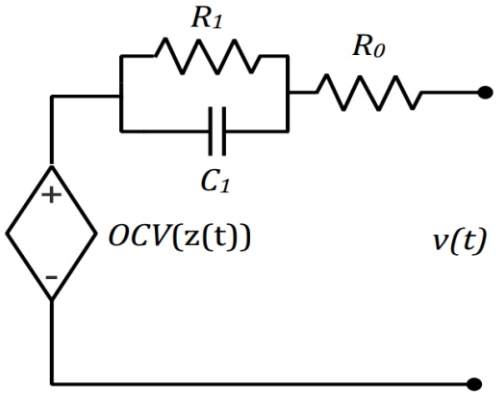

Figure 4. Cell model diagram including the polarization effect.

In this model, the state of charge equation remains the same as before, but the voltage equation changes:In continuous time:

$$v(t) = OCV\big(z(t)\big) - R_0 i(t) - R_1 i_{R_1}(t) \#(7)$$

In discrete time:

$$v[k] = OCV(z[k]) - R_0 i[k] - R_1 i_{R_1}[k] \#(8)$$

To find the current flowing in resistor R1, we write the expression for the total current:

$$i(t) = R_1 i(t) + C_1 \dot{v_{C_1}}(t). \#(9)$$

We replace $\dot{v_{C_1}}(t)$ by $\frac{R_1 d(i_{R1}(t))}{dt}$, we get the following differential equation

$$\frac{di_{R1}(t)}{dt} = -\frac{1}{R_1 C_1} i_{R1}(t) + \frac{1}{R_1 C_1} i(t). \#(10)$$

By converting this equation from continuous-time to discrete-time, we get:

$$i_{R_1}[k+1] = exp\left(\frac{-\Delta t}{R_1 C_1}\right) i_{R_1}[k] + \left(1 - exp\left(\frac{-\Delta t}{R_1 C_1}\right)\right) i[k]. \#(11)$$

Warburg impedance effect

The Warburg impedance models the diffusion of lithium ions in the electrodes. It depends on the frequency, modeled as ZW = AW/j where the constant AW is called the Warburg coefficient, and ω is the applied frequency in radians per second.

There is no simple differential equation to model Warburg's impedance. However, its effect can be estimated via several resistor-capacitor networks in series, using two distinct structures which are, the Cauer structure and the Foster structure.

Cauer's structure

Warburg impedance is represented by RC subcircuits as shown in figure (5)

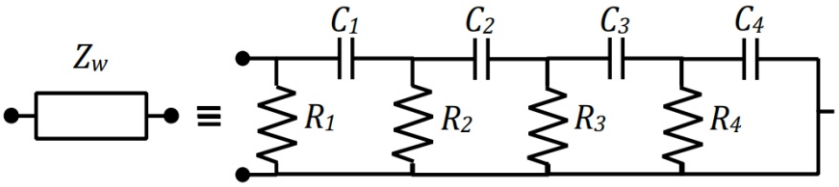

Figure 5. Cauer's structure diagram

Foster structure

In this case the impedance is only a set of RC circuits parallel in series as in figure (6):

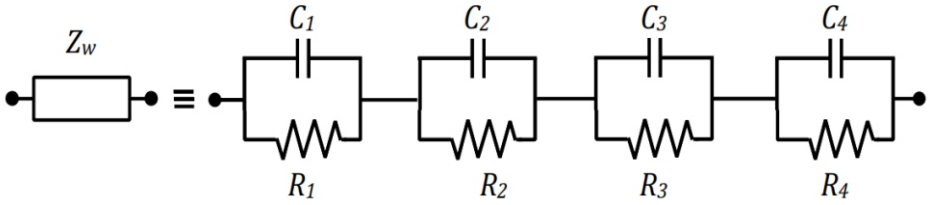

Figure 6. Foster's structure diagram

Hysteresis Effect

The model we have developed so far, implies that the voltage drop across R0 will immediately drop to zero when the cell current is zero, and the voltage drop across capacitor C1, will decrease to zero over time by discharging to resistor R1. In other words, the voltage across the cell will converge to the open circuit voltage OCV (z (t)).

However, the reality is something else. The cell voltage decreases to a slightly different value from the OCV, and the difference depends on the previous use of the cell. For example, we notice that if we discharge a cell at 50% SOC, and we leave it at rest, then the equilibrium voltage is lower than the OCV. On the contrary, if we charge a cell with 50% SOC, and we leave it at rest, then the equilibrium voltage is higher than the OCV. These observations indicate that there is a voltage hysteresis across the cell.

The hysteresis voltages are different from the diffusion voltage, the diffusion voltages change over time, on the other hand, the hysteresis voltages only change when the SOC changes. In addition, the hysteresis voltages are not directly related to time. This is because if a cell is allowed to rest, the diffusion voltages will decrease to zero, but the hysteresis voltages will not change at all.

There are two types of hysteresis, the first is the dynamic hysteresis which depends on the state of charge SOC, the other is the instantaneous hysteresis which results when the sign of the current changes (for example, the current change from cell discharge mode to cell charge mode).

Dynamic hysteresis

Let hD(z,t) be the dynamic hysteresis voltage as a function of SOC and time. The variation of this voltage as a function of the state of charge is described by the following differential equation:

$$\frac{dh_D\,(z,t)}{dz} = \gamma sgn(\dot{z})\big(M(z,\dot{z}) - h(z,t)\big). \#(12)$$

With:

M(z,ż) : Is a function which gives the maximum polarization due to the hysteresis as a function of SOC (z) and of the rate of change of SOC(˙).
The term M(z,ż) - h(z,t): indicates that the rate of change of the hysteresis voltage is proportional to the distance of the current hysteresis value from the main hysteresis loop.

The term γ, is a positive constant that regulates the rate of decay.

The term (˙) forces equation (12) to be stable for both charge and discharge of the cell.

To fit the differential equation of hD(z, t) in our model, it must be a differential equation with respect to time, and not with respect to SOC. And this is done by multiplying both sides of the equation by $\frac{dz}{dt}$:

$$\frac{dh_{\,D}(z,t)}{dz}\frac{dz}{dt} = \gamma sgn(\dot{z})\big(M(z,\dot{z}) - h_D(z,t)\big)\frac{dz}{dt}\ \#(13)$$

By replacing with:

$$\begin{cases} \dfrac{dz}{dt} = -\dfrac{\eta(t)i(t)}{Q} \\ \dfrac{dz}{dt}\,\mathrm{sgn}(\dot{z}) = |\dot{z}| \end{cases},$$

then we get the equation in continuous time:

$$\frac{dh_D\,(t)}{dt} = -\left|\frac{\gamma\eta(t)i(t)}{Q}\right| h_D(t) + \left|\frac{\gamma\eta(t)i(t)}{Q}\right| M(z,\dot{z}). \#(14)$$

By converting this equation into discrete time:

$$h_D[k+1] = exp\left(-\left|\frac{\gamma\eta[k]i[k]\Delta t}{Q}\right|\right)h_D[k] + \left(1 - exp\left(-\left|\frac{\gamma\eta[k]i[k]\Delta t}{Q}\right|\right)\right). \#(15)$$

have $M(z,\dot{z}) = -Msgn(i[k])$, and since $h_D[k]$ it is in volts, and $-M \le h_D[k] \le M$. It is useful to rewrite the equation in an equivalent representation but slightly different, which has a unitless hysteresis state $-1 \le h_D[k] \le 1$

$$h_D[k+1] = exp\left(-\left|\frac{\gamma\eta[k]i[k]\Delta t}{Q}\right|\right)h_D[k] - \left(1 - exp\left(-\left|\frac{\gamma\eta[k]i[k]\Delta t}{Q}\right|\right)\right)Msgn(i[k]) \quad (16)$$

Finally, the dynamic hysteresis is modeled as:

Dynamic hysteresis voltage $Mh_D[k]$

Instantaneous hysteresis

In addition to dynamic hysteresis which changes when SOC changes, we will model the instantaneous hysteresis voltage which changes when the sign of the current changes.

$$h_I[k] = \begin{cases} sgn(i[k]), |i[k]| > 0; \\ h_I[k-1], \quad \text{otherwise} \end{cases} \#(17)$$

Finally, the instantaneous hysteresis is modeled as:

Instantaneous hysteresis voltage = $M_0 h_I[k]$

In total, the overall hysteresis is:

$$M_0 h_I\,[k] + Mh_D\,[k]$$

Enhanced self-correcting the cell model

The Enhanced Self-Correcting (ESC) cell model combines all the elements already mentioned. The model is called Enhanced because it includes a description of the hysteresis, unlike some earlier models. The model is called self-correcting because the predicted terminal voltage of the model converges to the OCV plus the hysteresis when the cell is at rest, and converges to the OCV plus the hysteresis minus all resistive voltages at constant current. The final diagram of this model is shown in figure (7), which shows an example with a single resistor-capacitor pair in parallel. To compact the notation, we define a resistor-capacitor subcircuit speed factor $Fj = exp\left(-\frac{\Delta t}{R_i C_i}\right)$

$$i_R[k+1] = \underbrace{\begin{bmatrix} F_1 & 0 & \cdots \\ 0 & F_2 & \\ \vdots & & \ddots \end{bmatrix}}_{A_{RC}} i_R[k] + \underbrace{\begin{bmatrix} 1-F_1 \\ 1-F_2 \\ \vdots \end{bmatrix}}_{B_{RC}} i[k] \#(18)$$

So, if we define

$$A_H[\mathrm{k}] = \exp\left(-\left|\frac{\gamma\eta[k]i[k]\Delta t}{Q}\right|\right) h_D,$$

therefore, we will have the dynamic aspects of the model described by the following relation:

$$\begin{bmatrix} z[k+1] \\ i_R[k+1] \\ h[k+1] \end{bmatrix} = \begin{bmatrix} 1 & 0 & 0 \\ 0 & A_{RC} & 0 \\ 0 & 0 & A_H[\mathrm{k}] \end{bmatrix} \begin{bmatrix} z[k] \\ i_R[k] \\ h[k] \end{bmatrix} + \begin{bmatrix} -\frac{\eta[k]\Delta t}{Q} & 0 \\ B_{RC} & 0 \\ 0 & (A_H[k]-1) \end{bmatrix} \begin{bmatrix} i[k] \\ sgn(i[k]) \end{bmatrix} \#(19)$$

This is the equation of state of the ESC model. The output equation of the model is:

$$v[k] = OCV(z[k], T[k]) + M_0 h_I[k] + Mh_D[k] - \sum_j \mathrm{R_j i_{R_j}[k]} - \mathrm{R_0 i[k]} \ \#(20)$$

3. DETERMINING THE PARAMETERS OF THE CELL MODEL (ESC)

The model that we built describe two aspect of the cell, the first is static aspect of the cell, and the second is the dynamic aspect.

For the static aspect of the cell, this one is represented by open circuit voltage as a function of the state of charge, while another performance of the cell is dynamic. So, to determine the cell parameters. We do two kinds of experiments, the first one is where we determine the static aspect of the cell, here we charge and discharge the cell with a current almost equal to zero to minimize the excitation of the dynamic aspect of the cell. The second one is where we determine the dynamic aspect.

The data collected in the first experience are voltage values and ampere-hours charged and discharged in every step at different temperatures.

Determining the Coulombic efficiency

The Coulombic efficiency at 25°C :

$$\eta(25°C) = \frac{\text{total Ampere Hours discharged in all steps at 25C}}{\text{total Ampere Hours charged in all steps at 25C}}$$

The coulombic efficiency at temperature different than 25oC:

$$\eta(T) = \frac{\text{total AH discharged}}{\text{total AH charged in all steps at T}} - \eta(25°C) \times \frac{\text{total AH discharged in all steps at 25C}}{\text{total AH charged in all steps at 25C}}$$

*AH : Ampere-heurs

Determining of the relationship OCV versus SOC

Using the data collected from the experience, we will determine the relationship between OCV and SOC. However, the relationship that we will obtain is an approximate relationship, and that because the charge voltage and discharge voltage are different. So, in the high state of charge, we are forced to base OCV estimate on the discharge voltage values because we don't have any charge voltage information. While in the low states of charge we are forced to base the OCV estimate on the charge voltage values because we don't have discharge voltage information. In the intermediate state of charge, we can base OCV estimate on both charge and discharge values.

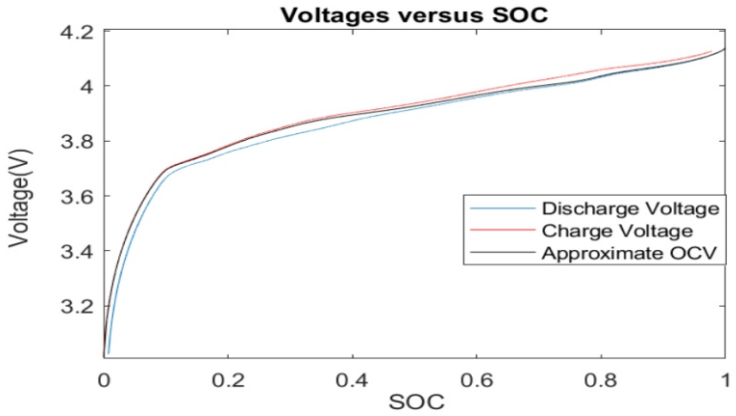

Figure 7. Open circuit voltage of the cell model based on data collected of discharge and charge OCV

This figure represents the approximate OCV/SOC relationship for a cell at room temperature. The black line is the approximate OCV, and the blue line is the discharge voltage curve, while the red line is the charge voltage curve. As we see, at high state of charge values, the OCV estimate is based on the discharge curve, while in the low state of charge, the OCV estimate is based on the charge voltage curve. In the intermediate states of charge, the OCV estimate is based on the two curves. The method used here to determine the OCV/SOC relationship at room temperature, is also used to determine it at all other temperatures of the experience.

Determining the dynamic parameters

Once we find the cell's OCV relationship, then we try to find the dynamic parameters of the cell model. This time, the cell must be exercised with profiles of current versus time that are representative of the final application of the resulting model.

Voltage values, current values, temperature values, ampere-hours charged, and ampere-hours discharged are recorded every second during the experience. These data are used to identify the cell model dynamic parameters. These parameters are; resistor value R1 and capacitor value R1 in the subcircuit, equivalent series resistor , hysteresis parameters and , hysteresis rate constant . Some of these parameters cannot be computed directly from the measured data, instead, we have to use an optimization approach, which we call system identification.

The simple way to do this is to choose a set of parameter values, the second step is to simulate the ESC model using that set of parameter values with the same input current as was measured during the experience, the third step is to compare the ESC model voltage prediction with the measured voltages, the fourth step is to modify the parameter values to improve the model prediction and go back to the second step and start again from there until the optimization is considered complete.

One approach used to determine the parameters of the cell model is to use an optimization toolbox such as MathWorks Simulink Design Optimization Toolbox. To do so, we must create a block diagram to implement the cell model equations. Figure (8) shows the implementation of ESC model in Simulink. For implementation we assume a model circuit with two parallel resistor–capacitor circuits $\eta = 1$, $\gamma = 3600$, and $M0 = 0$.

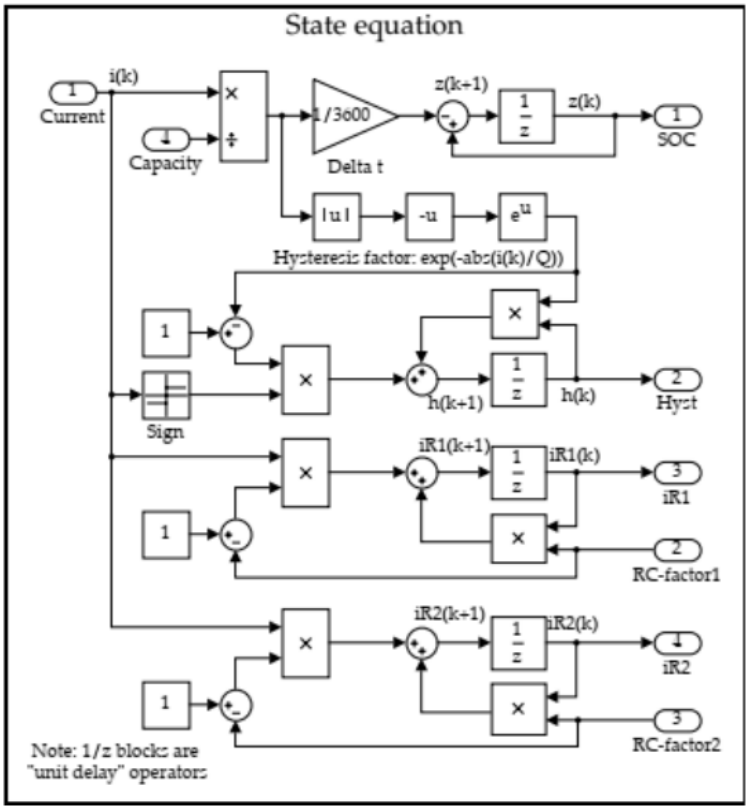

Figure 8. Block diagram of the Simulink Design Optimization Toolbox

This toolbox automatically generates values for cell capacitance, resistor-capacitor time constants, resistance values, and maximum hysteresis value, then runs the model to see how well the voltage predictions match the measured data. If there was a difference between the estimation and the measured data, we updateparameter's estimates, and repeats until it converges to a solution.
This method gives good results quickly if we initiate the parameter's value with good guesses. To do so, we try to compute directly some parameters values.

Direct computation of M, M0, R0, and Rj

The first thing to do before we go through the computation of the parameters, is to find the time constant of the resistor-capacitor circuits. Actually, the way to this is simple by using a method called system identification.

If we take a look at the output equation of the model, we will see that there are known parts such the ([ ] [ ]) ,and unknown parts which are the rest of the equation. We can rewrite equation 20 to distinguish known parts from unknown parts. [ ] can be computed directly from the current profile. To compute [ ] we require . For now, let's assume that we know its value. [ ] can be computed once know the resistor-capacitor time constant.

$$\tilde{v}[k] = v[k] - OCV(z[k], T[k]) \qquad \#(21)$$

$$= M_0 h_I[k] + M h_D[k] - \mathrm{R_j i_{R_j}[k]} - \mathrm{R_0 i[k]}$$

The variables h1[k],hD [k],iRJ[k],I [k] are input variables to equation (21). And the parameter's values can be computed as follows:

$$\underbrace{\tilde{v}[k]}_{Y} = \underbrace{\begin{bmatrix} h_I[k] & h_D[k] & \mathrm{i[k]} & \mathrm{i_{R_j}[k]} \end{bmatrix}}_{A} \underbrace{\begin{bmatrix} M_0 \\ M \\ \mathrm{R_0} \\ \mathrm{R_j} \end{bmatrix}}_{X}$$

We can find the unknown parameters vector via the least-square solution.

Optimization of γ

to find the parameters of the cell model, we assume that we know the value of in fact its value is unknown. So, we have to optimize it, to do that, we must bound it in some range, and then compute the quality of the fit for models optimized for each γ in this range, keeping only the model that offers the best quality of the fit.

4. CELL MODEL SIMULATION AND DISCUSSION

To give a better idea of the capabilities of our ESC model, we present some modeling results in this section. Data was collected from a 25 Ah automotive battery cell, and the open circuit voltage and dynamic modeling parameters were estimated from the data (using one sub-resistance-capacitor circuit in the model). Here, we focus on simulating the optimized model, where we compare its predictions with the voltage data measured for a test performed at 25 ◦C.

Figure 9 shows an overlay of the true voltage (blue line) and model predicted voltage (Orange line) over the entire 10-hour test. As we see in this figure there is fitness between measured voltage and predicted voltage. The root-mean-square difference between the actual results and the model results was 15.86 mV in this case. These results show more clearly that the circuit model captures cell performance quite well. As we see in figure 10, the error of the modeling is slightly small, the range of the error is between negative 0.1 and positve 0.1, this error depends on founded parameters values, but if somehow, we get a better value of those parameters this error will eventually decrease.

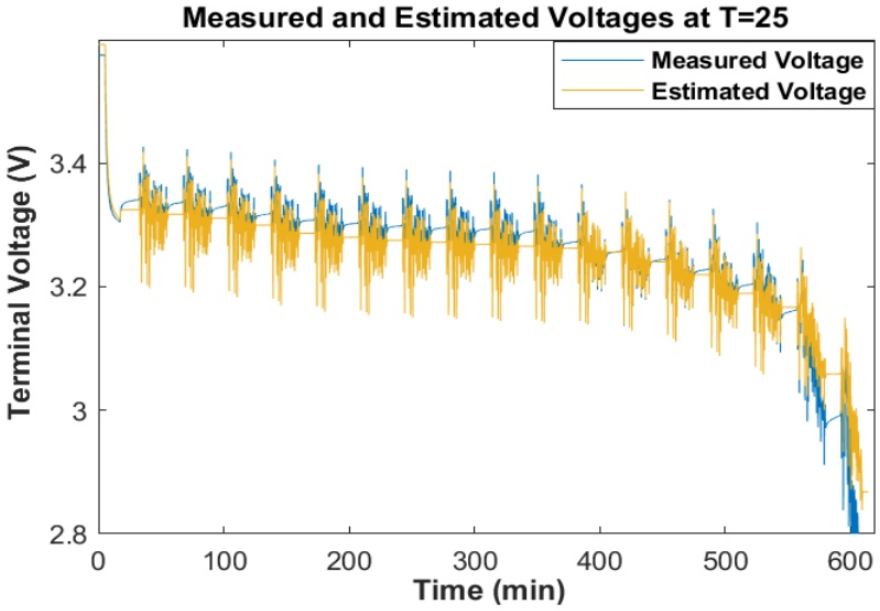

Figure 9. Cell measured voltage and cell model estimated voltage simulation versus time

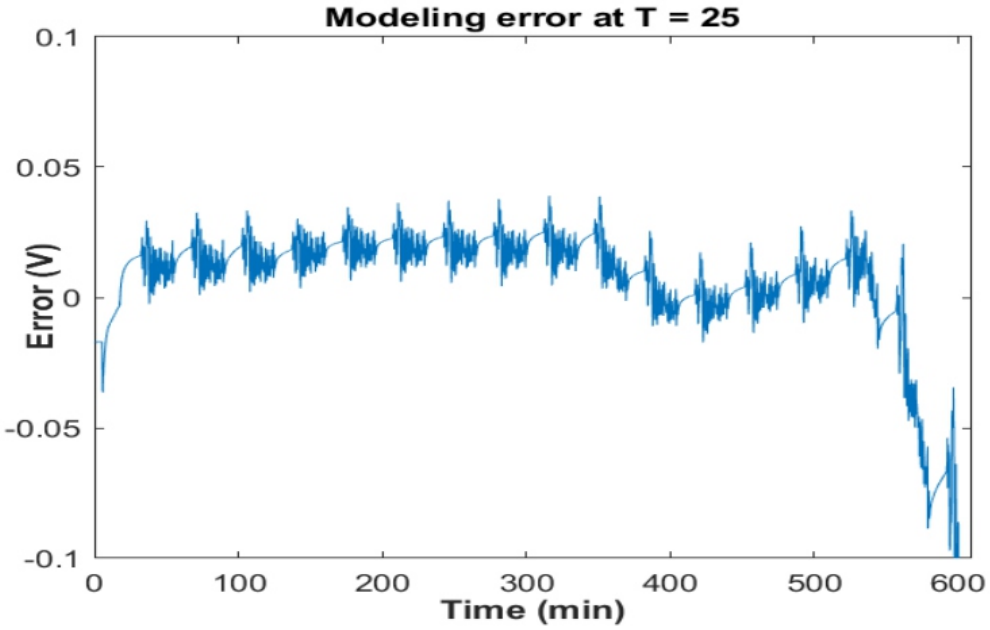

Figure 10. Error of the simulation versus time

Figures 11 show the optimized parameter values for this cell based on the test temperature (tests were performed from -25◦C to 45◦C in 10◦C increments).

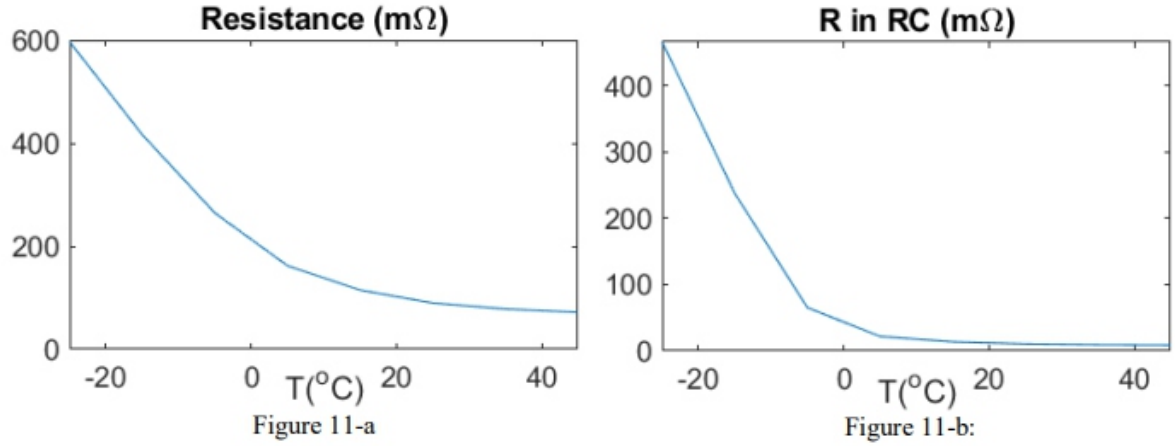

Figure 11-a

Figure 11-b:

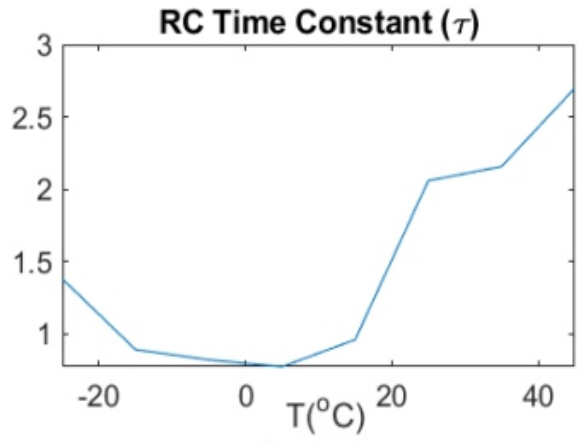

Figure 11-c

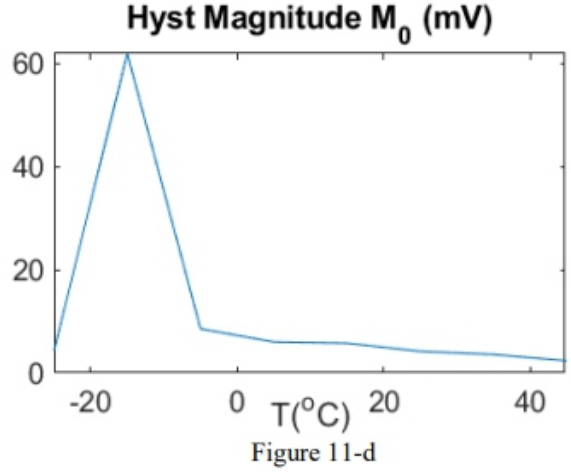

Figure 11-d

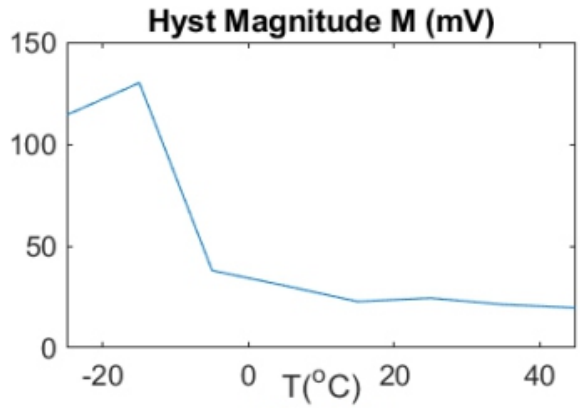

Figure 11-e

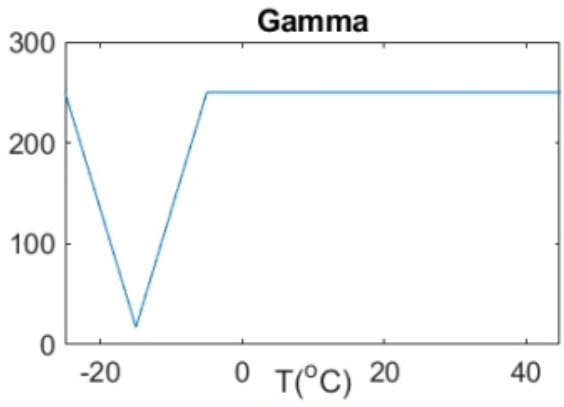

Figure 11-f

Figure 11-a shows serie resistance R0 evolution as function of temperature. the equivalent series resistance R0 decreases exponentially as the temperature increases. It is almost a universal result.

Figure 11-b shows the resistance (in resistance-capacitor subcircuit) evolution as a function of temperature. The resistor-capacitor resistances Rj tend to decrease exponentially as the temperature increases.This is also expected.

Figure 11-c shows the resistance-capacitor time constant evolution as a function of temperature. The resistor–capacitor time constants tend to increase with temperature increase. This might actually seem a surprising result, as we would expect the cell dynamics to speed up at warmer temperatures.

Figures (11-d, 11-e, 11-f) shows the hysteresis parameters evolution as a function of temperature and hysteresis time constant evolution as function of temperature. The Hysteresis is generally “speeding up” (i.e., a smaller change in SOC is required to effect a large change in the hysteresis state) and decreasing in magnitude as temperature increases. Hysteresis levels generally decrease as temperature increases.

In contrast to other cell models such as mathematical models, electrochemical models, thermal models, this model is intuitive and easy to impliment. This model uses only passive components such as resistors and capacitors and a voltage source, which they are suitable for use in circuit simulators. The accuracy of prediction and estimation achievable with this model is sufficient for many applications.

5. CONCLUSION

In this paper we built our model (ESC) using an electric analogy, our model can describe the behavior of the cell. Using a set of data collected from an application of the cell, we simulated our model and we compared the predicted voltage and measured voltage and we did find that our model predicts terminal voltage very well. The error of the modeling depends on the parameter’s values of the cell model and the measured data.

6. REFERENCES

[1] Wang, Y., Tian, J., Sun, Z., Wang, L., Xu, R., Li, M., & Chen, Z. (2020), "A comprehensive review of battery modeling and state estimation approaches for advanced battery management systems, "Renewable and Sustainable Energy Reviews, Volume 131, 110015.

[2] Zhang, R.; Xia, B.; Li, B.; Lai, Y.; Zheng, W.; Wang, H.; Wang, W.; Wang, M. " Study on the

Characteristics of a High-Capacity Nickel Manganese Cobalt Oxide (NMC) Lithium-Ion Battery—An Experimental Investigation," Energies 2018, 11, 2275.
[3] Xiaosong Hu, Haifu Jiang, Fei Feng, Bo Liu, " An enhanced multi-state estimation hierarchy for advanced lithium-ion battery management, " Applied Energy, Volume 257, 114019, 2020.
[4] Prashant Shrivastava, Tey Kok Soon, Mohd Yamani Idna Bin Idris, Saad Mekhilef, "Overview of model-based online state-of-charge estimation using Kalman filter family for lithium-ion batteries, " Renewable and Sustainable Energy Reviews, Volume 113, 109233, 2019.
[5] Cheng Chen, Rui Xiong, Ruixin Yang, Weixiang Shen, Fengchun Sun, "State-of-charge estimation of lithium-ion battery using an improved neural network model and extended Kalman filter, " Journal of Cleaner Production, Volume 234, Pages 1153-1164, 2019.
[6] C. Wei, M. Benosman, and T. Kim, "Online Parameter Identification for State of Power Prediction of Lithium-ion Batteries in Electric Vehicles Using Extremum Seeking, " Int. J. Control Autom. Syst., vol. 17, no. 11, pp. 2906–2916, Nov. 2019.
[7] A. Wen, J. Meng, J. Peng, L. Cai, and Q. Xiao, "Online Parameter Identification of the Lithium-Ion Battery with Refined Instrumental Variable Estimation, " Complexity, vol. 2020, p. 8854618, 2020.
[8] Huo, YT, Hu, W, Li, Z, Rao, Z, "Research on parameter identification and state of charge estimation of improved equivalent circuit model of Li-ion battery based on temperature effects for battery thermal management, " Int J Energy Res, Volume 44, Pages 11583– 11596, 2020.
[9] Qi Zhang, Yunlong Shang, Yan Li, Naxin Cui, Bin Duan, Chenghui Zhang, "A novel fractional variable order equivalent circuit model and parameter identification of electric vehicle Li-ion batteries," ISA Transactions, Volume 97, Pages 448-457, 2020.
[10] A. Gismero, D. -I. Stroe and E. Schaltz, "Comparative Study of State of Charge Estimation Under Different Open Circuit Voltage Test Conditions for Lithium-Ion Batteries," IECON 2020 The 46th Annual Conference of the IEEE Industrial Electronics Society, Singapore, 2020, pp. 1767-1772.

Instructions for Authors

Essentials for Publishing in this Journal

1 Submitted articles should not have been previously published or be currently under consideration for publication elsewhere.

2 Conference papers may only be submitted if the paper has been completely re-written (taken to mean more than 50%) and the author has cleared any necessary permission with the copyright owner if it has been previously copyrighted.

3 All our articles are refereed through a double-blind process.

4 All authors must declare they have read and agreed to the content of the submitted article and must sign a declaration correspond to the originality of the article.

Submission Process

All articles for this journal must be submitted using our online submissions system. http://enrichedpub.com/ . Please use the Submit Your Article link in the Author Service area.

Manuscript Guidelines

The instructions to authors about the article preparation for publication in the Manuscripts are submitted online, through the e-Ur (Electronic editing) system, developed by **Enriched Publications Pvt. Ltd**. The article should contain the abstract with keywords, introduction, body, conclusion, references and the summary in English language (without heading and subheading enumeration). The article length should not exceed 16 pages of A4 paper format.

Title

The title should be informative. It is in both Journal's and author's best interest to use terms suitable. For indexing and word search. If there are no such terms in the title, the author is strongly advised to add a subtitle. The title should be given in English as well. The titles precede the abstract and the summary in an appropriate language.

Letterhead Title

The letterhead title is given at a top of each page for easier identification of article copies in an Electronic form in particular. It contains the author's surname and first name initial .article title, journal title and collation (year, volume, and issue, first and last page). The journal and article titles can be given in a shortened form.

Author's Name

Full name(s) of author(s) should be used. It is advisable to give the middle initial. Names are given in their original form.

Contact Details

The postal address or the e-mail address of the author (usually of the first one if there are more Authors) is given in the footnote at the bottom of the first page.

Type of Articles

Classification of articles is a duty of the editorial staff and is of special importance. Referees and the members of the editorial staff, or section editors, can propose a category, but the editor-in-chief has the sole responsibility for their classification. Journal articles are classified as follows:

Scientific articles:

1. Original scientific paper (giving the previously unpublished results of the author's own research based on management methods).

2. Survey paper (giving an original, detailed and critical view of a research problem or an area to which the author has made a contribution visible through his self-citation);

3. Short or preliminary communication (original management paper of full format but of a smaller extent or of a preliminary character);

4. Scientific critique or forum (discussion on a particular scientific topic, based exclusively on management argumentation) and commentaries. Exceptionally, in particular areas, a scientific paper in the Journal can be in a form of a monograph or a critical edition of scientific data (historical, archival, lexicographic, bibliographic, data survey, etc.) which were unknown or hardly accessible for scientific research.

Professional articles:

1. Professional paper (contribution offering experience useful for improvement of professional practice but not necessarily based on scientific methods);
2. Informative contribution (editorial, commentary, etc.);
3. Review (of a book, software, case study, scientific event, etc.)

Language

The article should be in English. The grammar and style of the article should be of good quality. The systematized text should be without abbreviations (except standard ones). All measurements must be in SI units. The sequence of formulae is denoted in Arabic numerals in parentheses on the right-hand side.

Abstract and Summary

An abstract is a concise informative presentation of the article content for fast and accurate Evaluation of its relevance. It is both in the Editorial Office's and the author's best interest for an abstract to contain terms often used for indexing and article search. The abstract describes the purpose of the study and the methods, outlines the findings and state the conclusions. A 100- to 250-Word abstract should be placed between the title and the keywords with the body text to follow. Besides an abstract are advised to have a summary in English, at the end of the article, after the Reference list. The summary should be structured and long up to 1/10 of the article length (it is more extensive than the abstract).

Keywords

Keywords are terms or phrases showing adequately the article content for indexing and search purposes. They should be allocated heaving in mind widely accepted international sources (index, dictionary or thesaurus), such as the Web of Science keyword list for science in general. The higher their usage frequency is the better. Up to 10 keywords immediately follow the abstract and the summary, in respective languages.

Acknowledgements

The name and the number of the project or programmed within which the article was realized is given in a separate note at the bottom of the first page together with the name of the institution which financially supported the project or programmed.

Tables and Illustrations

All the captions should be in the original language as well as in English, together with the texts in illustrations if possible. Tables are typed in the same style as the text and are denoted by numerals at the top. Photographs and drawings, placed appropriately in the text, should be clear, precise and suitable for reproduction. Drawings should be created in Word or Corel.

Citation in the Text

Citation in the text must be uniform. When citing references in the text, use the reference number set in square brackets from the Reference list at the end of the article.

Footnotes

Footnotes are given at the bottom of the page with the text they refer to. They can contain less relevant details, additional explanations or used sources (e.g. scientific material, manuals). They cannot replace the cited literature.
The article should be accompanied with a cover letter with the information about the author(s): surname, middle initial, first name, and citizen personal number, rank, title, e-mail address, and affiliation address, home address including municipality, phone number in the office and at home (or a mobile phone number). The cover letter should state the type of the article and tell which illustrations are original and which are not.